The accretion of the Levant continental shelf alongside the Nile Delta by immense margin-parallel sediment transport

Elchanan Zucker, Zohar Gvirtzman, Didier Granjeon, Daniel Garcia-Castellanos, Yehouda Enzel

The accretion of the Levant continental shelf alongside the Nile Delta by immense margin-parallel sediment transport

Elchanan Zucker [1,2], Zohar Gvirtzman [1,2], Didier Granjeon [3], Daniel Garcia-Castellanos[4], Yehouda Enzel[1]

[1] The Fredy and Nadine Herrmann Institute of Earth Sciences, The Hebrew University of Jerusalem, Jerusalem 91904, Israel

[2] Geological Survey of Israel, Yesha'yahu Leibowitz 32, Jerusalem, Israel

[3] Department of Geology-Geophysics-Geochemistry, IFP Energies nouvelles, 1 à 4 avenue de Bois, Préau, 92852 Rueil-Malmaison, France

[4] Instituto de Ciencias de la Tierra Jaume Almera, ICTJA-CSIC, Barcelona, Spain

ABSTRACT

Following the termination of the Messinian salinity crisis ~5.3 million years ago, massive sedimentation in the Eastern Mediterranean Sea formed the huge Nile Delta. Alongside delta propagation, a continental shelf was accreted along the Levant margin. For several decades it was assumed that these two sedimentary structures were closely connected. Levant shelf deposits are composed of Nile-derived sediments and present-day measurements show that sand is currently being transported alongshore from the Nile Delta to offshore Israel. This study reexamines the existing paradigm about sediment transport and shelf-delta connection. We show that longshore sand transport is just a small part of a much larger process termed here margin-parallel sediment transport (MPST). Sand is transported in a nearshore shallow-water belt where marine currents are highly energetic. At the same time, shale is transported at greater depths over the deeper shelf and

the continental slope where marine currents are weaker. To model the accretion of the Levant shelf alongside the Nile Delta we use a 3D, diffusion-based, stratigraphic modeling tool (DionisosFlow) with a new module representing MPST. Our results show that margin-parallel transport of silt and clay in the deeper waters accounts for the bulk of deposition offshore Israel and is responsible for the development of the Levant shelf. Moreover, though MPST has begun coevally with delta formation, massive accretion of the Levant shelf was delayed by 2-3 My. Initially, a continental shelf formed offshore Sinai, then offshore Israel, and most recently along the Lebanon coast. Our model also demonstrates the significant lithological differences observed between sedimentation in front of the Nile River mouth and along adjacent continental margin. High energy down slope sediment transport carries sand, silt, and clay, whereas margin-parallel currents are relatively weak and carry mainly silt and clay. One exception within the margin-parallel system is the highly energetic nearshore current that transports sand. Thus, we point out, MPST is an efficient separator between shale and sand.

INTRODUCTION

The Nile Delta and its associated sedimentary cone are the largest in the Mediterranean Sea and one of the largest worldwide (Fig. 1). Five and a half million years ago, during the Messinian salinity crisis (Hsü et al., 1973; Ryan and Cita, 1978), the Mediterranean sea-level dropped and an approximately 1.5-km deep canyon (EoNile) incised into the Egyptian continental margin of the Mediterranean (Barber, 1981; Said, 1981; Fig. 2A). After this crisis, at the beginning of the Pliocene (5.3 Ma), when normal marine conditions resumed, sediments quickly filled this EoNile canyon and prograded from the canyon mouth into the open sea (Said, 1981; Sestini, 1989; Stanley and Warne, 1998). Today, after 5.3 My of progradation, the modern Nile Delta and its deep-sea

fan and sedimentary cone spread ~200 km Northward from the ancient canyon mouth and ~400 km in an east-west direction (Fig. 1). The thickness of the Pliocene-Quaternary (PQ) sediments building the Nile Delta and cone reaches ~4000 m in its depocenter offshore Egypt (Fig. 2B).

Alongside this PQ delta development, a continental shelf was accreted in the southeastern Mediterranean, offshore Sinai and Israel (termed here the Levant shelf, Fig. 1). The shelf deposits offshore Israel are composed of Nile-derived sediments. It was hypothesized that the accretions of both these features are coeval (Buchbinder and Gvirtzman, 1976; Emery et al., 1960; Gvirtzman, 1970; Nachmias, 1969; Shukri, 1950; Shukri and Philip, 1960). Using sedimentological and seismic data, numerous studies support that sediment transport is in a coast-parallel direction (Buchbinder et al., 1993; Carmel et al., 1985; Davis et al., 2012; El Din and Mahar, 1997; Emery et al., 1960; Emery and Bentor, 1960; Goldsmith and Golik, 1980; Golik et al., 1999; Golik, 2002, 1997, 1993; Klein et al., 2007; Manohar, 1981; Perlin and Kit, 1999; Schattner et al., 2015; Schattner and Lazar, 2016; Shoshany et al., 1996; Stanley, 1989; Zaghloul et al., 1982; Zviely et al., 2007, 2006). In addition, present day measurements and estimations of sediment fluxes indicate that effective longshore transport delivers large amounts of sand mainly northwards along the Nile-Levant littoral cell (e.g., Rosentraub and Brenner, 2007; Zviely et al., 2007 and references within). These observations and summaries have focused most of the research for several decades on the near-shore sand transport (Fig. 1, Black arrows).

However, as new observations for the relative young age (mainly Pleistocene) of the Levant continental shelf become available (Bar, 2009; Bar et al., 2013; Ben-Zeev and Gvirtzman, 2019; Elfassi et al., 2019), we question this existing view. If the Levant shelf coevolved alongside the Nile cone, why did its accretion start much later? The answer to this question presents major implications for understanding sediment transport along continental margins, in general, and

particularly to the sedimentary source of the Levant shelf. Since current sediments moving over the Levant shelf do derive from the Nile Delta, what are the main controlling processes that transport sediments along the continental margin and what types of sediments are transported by these processes?

In what follows we develop, first the concept, and then the quantification of margin-parallel sediment transport (MPST) not limited to sand grain size and not limited to the nearshore belt. Earlier evidence regarding a mid-shelf mud-dominated belt shaped by oceanographic processes, were documented in the Gulf of Lions at the mouth of the Rhone River (Rabineau et al., 2005; and references therein) and suggested for the Levant margins by Schattner et al. (2015). Here, we further develop this concept exploring the hypothesis that deeper and distal currents first conveyed large amounts of clays and silts along the ancient continental margin and only then, after generating this clay and silt foundation, the shelf was established on top with sand transport, as we see it today. I.e., we hypothesize that only after filling the quite large accommodation space with the finer grains and generating the shallow water environment, sand could have started to accumulate as we observe today on the present-day shelf.

Here, we test this hypothesis using the stratigraphic simulation software DionisosFlow (Granjeon, 1997, 2014; Granjeon and Joseph, 1999). DionisosFlow is a state-of-the-art, 3-D stratigraphic modeling tool that produces synthetic stratigraphy according to prescribed subsidence history, sea-level variations, sediment supply, water discharge, and sediment distribution by diffusion. The problem is that to date, DionisosFlow has no module to simulate margin-parallel transport at shallow (alongshore) or deep (off shelf) waters. Therefore, we added to it a new module that may answer some of the above questions. The new module includes a simple advection law in which sediment flux is defined by the user, and deposition rate is calculated from this flux accounting for

mass conservation. This volumetric exercise is constrained by ages and thicknesses of units. The sediment flux maps obtained by trial and error, indicate how much sediments pass through each point in the basin at various modelled time steps.

To account for lithological variations across the margin we also develop a depth-dependent function for the sand/shale ratio for the deposited sediments and the resulting stratigraphic section is calibrated by well data. Our results in terms of sediment flux and sand/shale ratio can be the basis for future physically based simulations that can better examine how surficial, intermediate, and deep marine currents transport sand and shale along various prescribed morphologies of continental margins.

GEOLOGICAL BACKGROUND

Sediment transport along the Nile littoral cell

The Nile littoral cell is one of the longest in the world with shorelines extending along ~700 km from the Nile Delta to northern Israel (Inman and Brush, 1973; Inman and Jenkins, 1984). The source of this littoral cell is in the Nile River, it passes along the shallow (up to 30 m deep) nearshore water belt of the Levant, with current northernmost terminal deposition at the Haifa Bay (Buchbinder et al., 1993; Carmel et al., 1985; and the other references quoted in the above introduction). Some sediments that are transported northward turn west, fall off the shelf and then deposited along the continental slope of the Levant (Ben-Gai et al., 2005; Schattner et al., 2015; Schattner and Lazar, 2016; see data about Units 3-4 below). In addition to the nearshore transport, Woodward et al. (2007) showed that present-day Nile sediments extend across the Levant and Herodotus basins as far as Rhodes, Crete and north of Cyprus.

Longshore transport usually refers to the net movement of coastal and nearshore sand parallel to the shore (Seymour, 2005). This transport is either by currents carrying sand in suspension or by waves on the seabed (i.e., bedload transport). It is easier to measure concentration of suspended sediment, but quite difficult to measure the bedload component. Quantitative estimates of longshore transport, therefore, are based commonly on inferences from the suspended sediment concentrations indicating that longshore transport is at a maximum under the breaking waves and in the swash zone on the beach face (Seymour, 2005).

The annual longshore flux of sand from the Nile Delta (Fig. 1) eastward is estimated at about 10^6 m^3 yr^{-1} (Inman et al., 1993, 1976; Inman and Jenkins, 1984). Offshore Sinai, this flux slightly decreases to ~$8.5x10^5$ m^3 yr^{-1} and ~$7x10^5$ m^3 yr^{-1} off Port Said and off El Arish, respectively (Inman et al., 1976). This flux is estimated at $4.5x10^5$ m^3 yr^{-1} and ~10^5 m^3 yr^{-1} at Ashkelon and Herzlia (Fig. 1), respectively (Perlin and Kit, 1999). Only a small portion (~$8.5x10^4$ m^3 yr^{-1}) of the initial sand flux reaches the currently considered final sink at Haifa Bay (Zviely et al., 2007).

Different Hypotheses

An important point was raised by Schattner et al. (2015) who argued that longshore transport is limited to the shallow (<30 m depth) and narrow (350-400 m) near-shore belt and cannot explain the deposition at greater depths. In addition, we stress that longshore transport only moves sand and silt, whereas the PQ shelf is mainly composed of shales (Yafo Formation) with only its topmost part composed of sand (Kurkar Group, e.g., Gvirtzman and Buchbinder, 1978).

Based on bathymetric, seismic, and oceanographic data, Schattner et al. (2015) suggest that since the Pleistocene-Holocene transition (~11 ka) fast water currents, termed the Levant Jet System (LJS; Fig. 1, red arrows), mobilizes sediments along the continental margin not only nearshore, but also in intermediate and deep waters (between 0 and 400 m water depths).

Timing of the Levant shelf accretion

A general PQ age was assigned for the continental shelf offshore Israel (e.g., Ben-Avraham, 1978; Ben-Gai et al., 2005; Gvirtzman and Buchbinder, 1978; Tibor et al., 1992). However, recent reexaminations of the biostratigraphy led Bar et al. (2009) to propose that most of the shelf was accreted later and that is composed primarily of Pleistocene sediments. This relatively young age is supported by Elfassi et al. (2019) and Ben-Zeev and Gvirtzman (2020) who demonstrate that after the Pliocene the pattern of sedimentation in the Levant Basin changed drastically; from thicker accumulation in the deep basin to thicker accumulation along the continental margin. Particularly interesting and crucial is the observation that the preferred deposition along the margin was delayed by 2-3 My after the commencement of the Nile Delta formation offshore Egypt (Ben Zeev and Gvirtzman, 2020). This, once more, raises the question why did margin-parallel sediment transport and shelf accretion begun so late? Why were sediments not transported along the Sinai-Israel margin already during their initial supply in the Pliocene?

Hypothetically, this can be answered by proposing that external forcing such as climate or ocean circulation could have triggered margin-parallel marine currents only in the Pleistocene. Alternatively, we hypothesize here, sediment transport along continental margins is a strong depth-dependent process that becomes more effective under certain bathymetry conditions. In the case of the Nile, we hypothesize that only after 2-3 My of delta accretion, the continental margin offshore Sinai could have become an effective conduit for sediment transport and large amounts of sediments started arriving to offshore Israel.

METHODS

Diffusion modeling in sediment transport

Since the early work of Culling (1960) and Young et al. (1973) and with the lack of specific information on the actual terms in physical sedimentology processes, diffusion laws have been used in geomorphology and geology to represent large-scale, spatially-averaged transport of sediment by creep, overland flow, and channel flow (e.g., Begin et al., 1981; Paola et al., 1992). Diffusive sediment transport states that the transport capacity of a water flow is proportional to the local basin slope and water discharge. It has been used in modeling sediment transport along alluvial fans, rivers and floodplains (Begin et al., 1981; Ben Moshe et al., 2008; Coulthard, 1999; Murray and Paola, 1994; Parker et al., 1998), mountains, foreland basins (Jordan and Flemings, 1991; Tucker and Slingerland, 1994) and passive margins (Rabineau et al., 2005).

Since the 1980s, when seabed morphology was shown to resemble lowland landscapes (e.g., Adams et al., 1998; Galloway, 1998; Mitchell and Huthnance, 2007; Schlager and Adams, 2001), laws of landscape evolution were extended to simulating progradation of deltas (Kenyon and Turcotte, 1985) and continental shelves (Granjeon, 1997; e.g., Jordan and Flemings, 1991; Kaufman et al., 1991; Mitchell and Huthnance, 2008; Rivenæs, 1997).

DionisosFlow is a 3D stratigraphic forward modeling tool aiming to simulate geometry and facies of sedimentary units on a scale of several tens to hundreds of kilometers and over geological intervals of 10^3-10^8 years (Granjeon, 2009; Granjeon and Joseph, 1999; Granjeon and Wolf, 2007); these are the scales of the problem at hand. At these spatial and temporal scales and the needed resolution, unfortunately, there is practically no way to apply physically based modeling. Using a diffusive approach for sediment transport (Gerber et al., 2009; Kaufman et al., 1991; Lai and Capart, 2007; Mitchell and Huthnance, 2008; Schlager and Adams, 2001; Spinewine et al., 2011; Steckler et al., 1999; Van Heijst et al., 2001), DionisosFlow averages the cumulative mass movement in time steps that combine many individual flows. In this way, DionisosFlow, for

example, ignores individual turbidites, but considers their cumulative mass movement. Similarly, and important for our study, it does not account for the discontinuity between fluvial and submarine systems in cases that sediments temporarily settle down on the delta front or inner shelf and only later are transported downslope by gravity-driven processes. For simplicity, it assumes that flows continue seaward either directly by hyperpycnal flow or by slope failures.

DionisosFlow formulates two large-scale sedimentary processes: slow creep and fast transport driven by water discharge (Tucker and Slingerland, 1994; Willgoose et al., 1991). Creep is simulated by a linear, slope-driven diffusion equation (i.e., transport is proportional to gradient). Water-driven flow is simulated by a non-linear water- and slope-driven diffusion equation. Combining the driving equations of these transport laws (Granjeon, 2014; Granjeon and Joseph, 1999) leads to the sediment transport equation:

$$Q_S = -(K_s + K_w Q_w^n S^{m-1})\, \vec{\nabla}\, h \qquad (1)$$

Where Q_s is sediment flux [km^2/yr]; h [m] is topographic elevation; K_s and K_w [km^2/yr] are the diffusion coefficient, respectively for slow creep transport and water flow process; Q_w is dimensionless local water discharge at the cell; S is local gradient of basin slope; n and m are constants, usually ranging between 1 and 2. Transport equation and mass conservation are applied to each grain size, leading to definition of local sedimentation or erosion. Sedimentation occurs where transport capacity decreases (by decreasing gradient or slower water flow) and erosion occurs where transport capacity increases.

The capability of DionisosFlow to simulate the production of large-scale systems such as deltas, fluvial plains, shelf plains, incised valleys, and deep water systems was tested and validated in several studies including, for example: (1) the XES 02 flume experiments designed to reproduce

fluvial plain and incised valleys (Granjeon, 2014); (2) Synthetic case studies built to investigate the impact of millennial-scale climatic and eustatic cycles on the growth of a delta and the associated fluvial channel belts and incised valleys (Csato et al., 2014; Rabineau et al., 2006, 2005); (3) On modern delta, shelf, and deep-water turbiditic systems such as the Niger Delta (Laurent et al., 2020) and the Orinoco deep-sea fans (Deville et al., 2015).

Simulating margin-parallel sediment transport

The margin-parallel transport module developed here begins with a sediment flux map describing the intensity [km^2/My] of the flux transported through a given location in a coast-parallel, dynamically updated direction, which evolves with time. The flux obeys a simple user-defined advection law that accounts for mass conservation, i.e., when the flux decreases, sediments depart from the suspension plume and deposit. The rate of deposition, SED [km/My] is:

$$\begin{cases} \overrightarrow{q_{mp}} = Q_{mp}(x,y)\ .\ \vec{n} \\ SED\ (x,y) = -div\ (\overrightarrow{q_{mp}}) \end{cases} \quad (2)$$

With q_{mp} the margin-parallel sediment flux [km^2/My], Q_{mp} the user-defined intensity of this flux, n a unit vector parallel to the closest shoreline [dimensionless], and SED [km/My] the sedimentation rate induced by this margin-parallel sediment transport.

The sand/shale ratio within the deposited sediment is computed from a given depth-dependent function, derived from observations. In addition to this deposition rule, we use the classical diffusion equations to transport sediments as soon as they reach the sea floor. By the end of this computation, we obtain a stratigraphic layer whose thickness is compared to observations. By trial-and-error (i.e., sensitivity over a range), the flux map is corrected, and simulations rerun until they satisfy borehole and geophysical observations.

Data

Basin structure

The stratigraphic PQ sequence simulated here is bounded by the present-day bathymetry at its top and the base Pliocene surface at its bottom. Bathymetry (Fig. 1) is taken from ETOPO1 (Amante and Eakins, 2009). The base Pliocene structure map (Fig. 2A) is after Zucker at al., (2019). The PQ isopach (Fig. 2B), which is the subtraction of Fig. 2A from Fig. 1, defines a major depocenter under the Nile Delta and cone (reaching a thickness of 4 km) and a secondary and connected, local depocenter under the Israeli coastal plain and shelf (reaching a thickness of 2 km). Resolving these two depocenters - a delta and an adjacent continental shelf - are the targets of this simulation.

Paleo-bathymetry

For the paleo-bathymetry at 5.3 Ma (Fig. 3A), which is the surface on which we begin to model deposition, we used the base Pliocene map corrected for the load of the overlying sediments (PQ section). For this flexural backstripping procedure, we assumed an average density of 2000 kg/m^3 for unloaded sediments, adopting a pure elastic thin plate approach to isostasy and an elastic thickness of 30 km, a relatively large value consistent with the old tectonothermal age of the northeast African margin. For the decompaction of the underlying sediments, we considered an approximately 10-km thick pre-Pliocene section. The decompaction results are very insensitive to the depth of the base of this layer because only the upper ~2 km retains a significant porosity. Details about this pseudo-3D (planform) flexural backstripping procedure are described in Garcia-Castellanos et al. (2003) and in Amadori et al. (2018). To correct for post-Miocene tectonics, the sediment-unloaded map was smoothed in the area of the Rosetta and Temsah faults (Fig. 2A),

which were active in the PQ (Aal et al., 2000). In addition, the northern Levant Basin that subsided towards the Cyprus Arc during the Plio-Quaternary (Ben-Avraham, 1978; Kempler, 1998; Robertson, 1998; Schattner, 2010) was uplifted by ~200 m. The uncertainty of post Miocene tectonics is discussed below.

Subsidence

Subsidence (Fig. 3B) is calculated in the model by taking the difference between the paleobathymetry at 5.3 Ma (Fig. 3A) and the present-day base Pliocene surface (Fig. 2A), the surface which should be obtained at the end of simulation. Average subsidence rate for the entire simulation is taken as the total calculated subsidence divided by 5.3 My. This assures that at the end of the simulation, the modeled and observed base Pliocene surfaces will coincide to allow comparing the modeled and observed bathymetries (Fig. 3C).

Sediment supply

A first order approximation for sediment supply is derived from the total volume of the PQ isopach (Fig. 2B) divided by 5 million years (i.e., 70,330 km^3/My). From this number we subtract biogenic carbonates produced in the water column. Well samples and logs from the Israeli coastal plain indicate that the Plio-Quaternary Yafo Formation contains ~10% calcite in the form of micro- and nano-fossils (Gvirtzman, 1970). Considering that 10% of the total PQ volume did not arrive from the clastic feeders, we initially applied 90% of the total deposited volume. After a set of trials constrained by the sediment thickness maps, we applied an average value of 64,417 km^3/My (~91.5%) to represent sediment supply by the Nile River for the entire duration of the model. It is interesting to note that this average value obtained from sediment volume is on the same order of magnitude as the sediment yield presently measured at the mouth of the Nile River (60,000

km^3/My, Syvitski and Milliman, 2007). Sand/shale ratio for Nile sediments was taken as 20% and carbonate production was taken as 5,910 km^3/My.

Margin-parallel transport

Regarding present-day measurements of longshore transport (references above) it should be noted that they refer only to the sand fraction (1000 km^3/My from Nile Delta to Sinai; 850 km^3/My at Port Said, 700 km^3/My at El Arish; 450 km^3/My at Ashkelon; 100 km^3/My at Herzlia; and 85 km^3/My arrive to Haifa Bay). The big unknown in our simulation is the total amount of sediments (sand to clay) moving along the continental margin nearshore, on and off the shelf.

A lower limit for the total sediment flux along the Levant continental margin is obtained from the average deposition rate along the Israeli margin since the early Pliocene. Considering a rectangular 200 km (Rafah to Southern Lebanon) by 20 km (approximately the mean width of shelf) by 2 km (thickness of PQ section offshore Tel Aviv), the total volume of the Israeli shelf is about 8,000 km^3. Dividing this by 5.3 million years, yields ~1500 km^3/My. This set a minimal constraint for the flux that entered the Israeli margin from offshore Sinai, because the actual flux includes sediments that continued northward to offshore Lebanon. No siliclastic sediments can enter the shelf from the onshore carbonate platform of the Levant. It is interesting to note that this estimated minimum value of total sediment flux triples the sand flux (~500 km^3/My) currently entering to Israeli margins at Rafah (the southern boundary of the Gaza strip between El Arish and Ashkelon). Below, the unknown flux of sediments along the Levant continental margin is modeled by trial-and-error.

Water discharge

Present day water discharge of the Nile River is 2830 m^3/s (Milliman and Syvitski, 1992). The paleo-discharge of the ancient Nile River can be further, but only roughly, constrained by

paleogeographic (drainage area) and paleoclimatic (rain) considerations and compared with modern rivers worldwide that have similar drainage areas (Dai and Trenberth, 2002; Milliman and Syvitski, 1992; Syvitski and Milliman, 2007). Although we are aware of the impact of Quaternary climatic changes on the Nile discharge, for the lack of data and for the sake of simplicity, we took the present-day value as a constant throughout the entire duration of the model.

Diffusion coefficients

Efficiency of sediment transport depends on difficult-to-quantify factors such as grain size, lithology, roundness, water depth, water discharge, vegetation, river type and more. In practice, coefficients used to model various basins do not always express the same factors and their values vary greatly from case to case. One reason for this large range is that efficiency of diffusion can be controlled either by the diffusion coefficient or by the amount of water pushing the sediments (Equation 1). Accordingly, Gvirtzman et al. (2014) and Hawie et al. (2015) showed that by constraining water discharge, the range of possible diffusion coefficients is narrowed. Recent stratigraphic forward models run at a basin scale, using diffusion laws to simulate slow creep and water flow processes, and calibrated on seismic and well log data suggested the following range of values (Table 1): Ks (slow creep) is about 0.001 to 0.05 km^2/ky for sand, and 0.001 and 0.1 km^2/ky for shale; while Kw (water flow process) is about 50 to 2,000 km^2/ky for sand in terrestrial environments, 100 to 4,000 km^2/ky for shale in terrestrial environments, 0.01 to 20 km^2/ky for sand in marine environments, and 0.063 to 100 km^2/ky for shale in marine environments (Csato et al., 2014, 2013; Gvirtzman et al., 2014; Harris et al., 2016; Hawie et al., 2018, 2017; Zhang et al.,

2019). Here we take the present-day water discharge of the Nile as a starting point and identify the best-fit diffusion coefficients of shale and sand inside these ranges by trial and error.

Sand/shale ratio

Present-day measurements of sediment composition at the seabed offshore Israel (Almogi-Labin et al., 2012) indicate the presence of three coast-parallel belts (Fig. 4A): (a) An almost pure, well-sorted sand belt from the shoreline to a water depth of 35 m. (b) A silt-dominated belt from water depths of 35-100 m in which the amount of silt gradually grows from a few percent at a depth of 35 m to 85% at depths of 60-100 m. The rest is shale; this shale represents only a few percent of the total sediment volume near the coast and 10-15% at depths of 60-100 m. (c) A shale dominated belt at depths >100 m, where sand is negligible. For modeling we simplified these observations to only two components (sand and shale) with a depth-dependent ratio shown in Fig. 4B.

Modeling strategy

The first objective of this modeling study is to obtain the diffusion parameters that explain the Nile Delta formation with the given values of water discharge and sediment supply. For this, we first use DionisosFlow without the added new module of MPST. Considering that the base of the simulated PQ package is forced to coincide with the observed base Pliocene surface (see above constraints for subsidence), testing the model is carried out by comparing the modeled and observed bathymetries. If bathymetry fits, sediment thickness also fits. This stage of the modeling is expected to provide a rough fit between the model and observations at the delta area, but not at the Levant margin.

The second objective is to simulate the formation of the Levant shelf. For this, we apply all model parameters realized in the first stage (and particularly the diffusion coefficients) and rerun DionisosFlow; this time the runs include the upgraded module for margin-parallel transport. By numerous trial-and-error runs, we identify the sediment flux maps that yield the better fit between model and observation. For calibration of the lithostratigraphy, we use a published lithostratigraphic section that distinguishes the sandy Kurkar Group from the shales of the Yafo Formation (data from Gvirtzman and Buchbinder, 1978). For chronostratigraphic calibration, we use the subdivision of the PQ section offshore Israel identified for four dated seismic units (Ben-Zeev and Gvirtzman, 2019; Elfassi et al., 2019).

RESULTS

Stage 1: basic model without the margin-parallel sediment transport (MPST)

Fig. 5 presents the simulated bathymetry from 5.3 Ma to the present, using the basic model without the MPST. The parameters for sediment distribution that generate this model are listed in Table 1. These results demonstrate that the model successfully produces the Nile Delta, but essentially fails to produce the Levant shelf. The general fit between model and present-day observations in bathymetry and thickness (Fig. 6A) is evident in section AA' crossing the Nile Delta. Moreover, comparison to a published geological section in that area from Kellner et al. (2009) indicates that even the subdivision between Pliocene and Quaternary is modeled quite well (Fig. 6C). On the other hand, offshore Israel there is only a poor fit between model and observations (Fig. 7A, B). This discrepancy in the east-west cross sections is primarily because the model produces by far too little deposition offshore Israel (Fig. 8A). The map presenting the discrepancy in thickness between model and observations (Fig. 8B) further indicates that the sediment, unaccounted for at

the Levant margin (~2 km, blue colors), is compensated by excess sediments in the Herodotus Basin (200-900 m, red); i.e., the sediments were delivered there. This discrepancy strengthens our hypothesis that without a large margin-parallel sediment supply, it is impossible to simulate the formation of the Levant continental shelf.

Except for this discrepancy, which is related to the lack of margin-parallel transport, the generally good agreement between model and observations offshore the Nile Delta (e.g., Fig. 6) indicates that (1) sediment distribution in the model functions quite well, and (2) average values of Qw, Qs for the entire simulated interval are suitable approximations. We therefore take model parameters obtained in the first modeling stage and continue to the next stage.

Stage 2: Adding the margin-parallel sediment transport (MPST) to the model

Fig. 9 shows the simulated bathymetry from 5.3 Ma to the present, using the upgraded model, which includes the margin-parallel sediment transport (MPST) module. Unlike the basic model (Fig. 5), here with the addition of this module, a shallow continental shelf is produced (orange color) offshore Israel with nearly a 2-km-thick section deposited there (Fig. 10A). Throughout the studied area, the model produces a thickness within <200 m from the observed thickness (Fig. 10B); this is quite a satisfactory result as this value is within <10% of the total observed thickness. Two modeled chronostratigraphic cross sections offshore Caesarea and Ashdod demonstrate the good fit with observations (Fig. 11). Furthermore, Two lithological sections at the same location (Fig. 12) indicate that sand is accumulated only in the upper part of the section. This is also consistent with observations as the age of the Kurkar Group varies laterally, from Pliocene-Pleistocene inland to only Pleistocene at the coastline (Fig. 12C, Gvirtzman and Buchbinder, 1978). According to our model, farther west at the shelf area, the age of the sandy Kurkar Group

is limited to a few hundred thousands of years and to only several tens of thousands of years near the shelf edge (Fig. 12). The noticeable sand intercalations into the shaly section represent intervals of eustatically low sea levels (Haq et al., 1987) used as part of the model input.

The successful simulation of sand deposition and its accretion in the shallow environment is the outcome of the depth-dependent sand/shale ratio (Fig. 4) that was fed to the model. This depth dependency is also expressed in Fig. 13 and indicates that more sand was deposited offshore Israel during the latter part of stratigraphic sequence accretion (1.8-0 Ma), when a shallow shelf was already developed.

Rates, accretion, and shelf buildup

To summarize our results, we compare modeled and observed sedimentation rates in the Levant Basin over the four time intervals of 5.3-2.6 Ma, 2.6-1.8 Ma, 1.8-0.35 Ma, and 0.35-0 Ma (i.e., interval durations of 2.7, 0.8, 1.45, and 0.35 My), which were defined as traceable chronostratigraphic zones by Elfassi et al. (2019) based on seismic- and bio-stratigraphy. These four stratigraphic units are the basis for the four thickness maps prepared by Ben Zeev and Gvirtzman (2019) and are the basis for the rates we use in the comparison with the modeling. The division of the thickness of the four units corresponds to the above interval durations.

Deposition rates calculated for the basic model (without MPST), indicate that deposition was not sufficient to form a continental shelf in the Levant (Fig. 14). In the upgraded model that includes MPST a continental shelf is gradually built; this buildup is observed in the model to occur first, offshore Sinai, then offshore Israel, and most recently offshore Lebanon. The calculated rates of accretion are consistent with observations but present some exceptions. Unit 2 (Gelasian) in the actual stratigraphy presents an increase in sedimentation rate both in the southwest, near the Nile

Delta, and along the Levant margin (Fig. 14). This could have been an expression of a temporal increase of the Nile's sediment discharge, which we do not model. Furthermore, the Israel Slump Complex that provided ~1,000 km^3 of sediments from the Levant slope to the basin (Frey Martinez et al., 2005) in a short episode, limited to Unit 2 (Elfassi et al., 2019) and is not modelled either. In addition, our model ignores other local sediment contribution that may have reached the basin from the east (e.g., the Yafo sand member, Druckman et al., 1995; Frey-Martınez et al., 2007; Frey Martinez et al., 2005; Gardosh et al., 2009).

The importance of the MPST is demonstrated by comparing (Fig. 15) sedimentation rates in the deep basin and at the continental margin (locations appear as white dots in Fig. 14). In the basic model, without MPST, the difference between these two localities is minor and the rate of sedimentation is relatively low in both. This is because the model depends almost entirely on slow and gradual diffusion of sediments from the Nile Delta through and into the deep basin. On the other hand, with the addition of the MPST, increasingly more sediments arrive and deposit along the continental margin of the Levant and as a result less sediments reach and deposit in the deep basin.

Margin-parallel sediment flux

Sediment flux maps obtained by trial-and-error are shown in Fig. 16A-B. In these maps each pixel represents a flux (km^2My^{-1}) in a coast-parallel direction (approximately to the northeast). Integrating the pixels along an east-to-west transect across the continental margin, provides the total northward sediment flux (km^3My^{-1}) through that transect line (Fig. 16C-D).

During the first modeled interval (5.3-1.8 Ma), calculated sediment flux offshore Rafah was ~2500 km^3My^{-1} (Fig. 16D, blue line). Most of these sediments were trapped and deposited offshore Israel

while very little volume continued north of Haifa. This has changed during the 1.8-0 Ma interval with flux offshore Rafah reaching ~5,300 km^3My^{-1} and the flux offshore Haifa increased to ~3000 km^3My^{-1} (Fig. 16D, red line). Subtracting the modeled flux north of Haifa from the flux offshore Rafah indicates that about 2300 km^3My^{-1} of sediments were trapped in the shelf south of Haifa; this is not very different from the volume deposited during the first interval (2500 km^3My^{-1}).

The modelled total sediment fluxes are difficult to compare to present-day observations that measure only the sand flux, but they do produce satisfactory results for deposition and the quite correct thickness. Sand fluxes are easier to compare (Fig. 16C). They show that during the early interval less than 100 km^3My^{-1} had entered the Israeli margin from the south (Rafah) and these were trapped almost immediately (Fig. 16C, blue line). During the 1.8-0 Ma interval nearly 350 km^3My^{-1} of sand entered from offshore Rafah, most of it trapped before reaching Ashdod, and about 40 km^3My^{-1} of sand arrived at Haifa (Fig. 16C, red line). These results are slightly lower than the present-day observations and may be improved by a sensitivity analysis that will include changes in the sand/shale ratio considered in the model input. In general, approximately 6% of the modeled sediment flux offshore Israel is sand, concentrated in near coastal areas.

The two flux maps (Figs. 16A, 16B) indicate a northward shift of transport and alongshore deposition propagation between the first and second sequences. Initially sediments were primarily trapped offshore Sinai and only then offshore Israel. Moreover, during the first interval sediment transport offshore Israel occurred mainly at deep waters (i.e., west of the first isobath after isobath 0 m - isobaths 200 m in Fig. 16A), whereas during the second interval transport mostly occurred on the shelf (i.e., east of isobaths 200 m depth in Fig. 16B).

DISCUSSION

Continental shelves and river deltas

Development of continental shelves adjacent to river deltas is quite common, but the dependency of the shelf evolution on sediment transport from the nearby delta is not fully resolved. Here we study the accretion of the Levant shelf alongside the Nile Delta, exploring coevality and the dependency of the Levant shelf on sediment transport from the Nile Delta. First, we show that longshore sand transport is only a small fraction of a much larger process, termed here MPST. In the Levant shelf, sand accumulation in the past 5 My comprises only about 6% of the total volume of sediments that arrived from the Nile Delta. Furthermore, without the large transport of silt and clay in the deeper waters, deposition offshore Israel probably would have been negligible, and the Levant shelf never would have developed (Fig. 14).

Our observations and modelling results indicate that MPST has begun coevally with delta formation, but at first, developed quite slowly. Initially, a continental shelf formed offshore Sinai, then offshore Israel, and most recently along the Lebanon coast, where it is probably still in its initial buildup stage. Throughout this time, longshore sand transport and deposition has taken place near the coastline, but only recently (sometime in the last hundreds or tens of thousands of years), when the shelf became shallow enough, sand transport and deposition expanded westward. We hypothesize that this westward expansion was more pronounced during eustatic sea-level drops.

Our results emphasize the importance of deep-water, margin-parallel currents for sediment transport (e.g., Rebesco, 2018, 2005; Rebesco et al., 2014; Rebesco and Camerlenghi, 2008; Schattner and Lazar, 2016 and references within), which is studied less than longshore sand transport (see introduction) and is still poorly understood. The argument that sand transport along the Levant margin occurs within a wide depth range (0-400 m), was first proposed by Schattner et

al. (2015), arguing that sediments are transported by the Levant jet system (LJS), which is a fast water current related to the present day thermohaline circulation in the Eastern Mediterranean. According to Schattner et al. (2015) this jet system initiated during the Pleistocene-Holocene transition (~11 ka), intensifying after the last glacial maximum (LGM). Our results show that MPST started coevally with the Nile Delta formation (5.3 Ma) and intensified at the beginning of the Pleistocene (2.6 Ma). We do not have any knowledge of the water circulation during the Pliocene and Pleistocene. However, based on our knowledge of the depositional history, we infer the paleo-sediment fluxes. These fluxes indicate margin-parallel transport much earlier than the Holocene, even at depths greater than 400 m. At the nearest shore environments, where they are dependent on eustatic sea levels, it is possible that the last emplacement of the jet occurred following the last glacial. If the current interglacial is a clue to the past, this could have been a cyclic occurrence during the Quaternary with early interglacials experiencing an increase in Nile River discharge and sediment supply to its delta accompanied by pronounced LJS that intensified the MPST. Such a cyclic process may have facilitated the construction of the Levant continental shelf.

Obviously, our model is not driven by physical processes. However, it presents a first step in transforming available data about sediment deposition in and on shelves (thickness and lithology) into sediment fluxes. This is essential for future physically based simulations that can examine how surficial, intermediate, and deep marine currents transport sediments along various morphologies of continental margins.

Margin-parallel vs. margin-perpendicular sediment transport

In the Levant margin sand is forming a relatively thin sequence at the top of the shelf, reaching ~180 m at the coastline and wedging out landwards. Sand grains comprise 90-100% of this sequence (i.e., the Kurkar Group; Fig. 12). Conversely, sand is spread throughout the entire thickness (>3.5 km) of the PQ section of the Nile Delta, ; from its base to its top and from its eastern to western edges, comprising a maximum of 50% (Fig. 6B). We propose that this profound difference in sand content is an expression of the available energy for transport. Sediment flow from the river mouth straight down to the deep basin is stronger in comparison with margin-parallel flow that keeps a nearly constant elevation. Accordingly, offshore the Nile River mouth, sand grains were transported straight downslope over large distances since the early Pliocene. On the other hand, the much weaker margin-parallel currents transported only fine grains that had built the shaly Levant shelf. One exception within the margin-parallel system is the highly energetic nearshore current that transported sand continuously since the Pliocene. This, however, is limited, here and probably elsewhere, to a very narrow zone and very shallow water depth. Thus, the combination of near shore energetic currents and deeper weaker currents produce an efficient differentiation between shale and sand deposits, although they source at the same river mouth. Such differentiation characterizes margin-parallel sub-horizontal sediment transport in contrast with the margin-perpendicular steep-gradient transport.

An additional basin-wide expression of the margin-parallel vs. the common margin-perpendicular transport is deltas growing thicker towards the open sea more than they grow wider along the adjacent continental margins. The Nile Delta started developing immediately following the recovery from the Messinian salinity crisis (early Pliocene) and then it had propagated 150-200 km from the river mouth northward within about 1 My (Fig. 9). At the

same time the Levant coast started receiving small amounts of sand (Pleshet Formation, Gvirtzman and Buchbinder, 1969). The shelf, which has existed earlier (probably was initially forming in the Miocene) presumably was very narrow (Buchbinder and Zilberman, 1997; Gvirtzman and Buchbinder, 1969). Only 2-3 My after the beginning of delta formation a notable shelf began developing in the Levant margin (Figs. 9, 11).

Implications for shelf exposure during sea level drops

The youngest stage (tens or hundreds of thousands of years) of delta development is the extension of sand deposition 10-20 km westward during eustatic lowstands (Fig. 13). These results are consistent with the proposal of Amit et al. (2011) that only around 180-200 ky, the Nile Delta has been accreted to levels that its surface could have been exposed during eustatic low stands. Only then, the sand surface and deposits of the delta and the northern Sinai shelf could have been subaerially exposed and initiate their eolian transport under the windy glacial climate in northern Sinai. This sand transport has generated the northern Sinai dune fields and abraded the sand grains into coarse silts that comprise the loess of the Negev (Amit et al., 2011; Crouvi et al., 2008). We hypothesize that some of the shelf sand was also exposed and was involved in the accretion of the Eastern Mediterranean coastal plain (Harel et al., 2017).

CONCLUSIONS

1. Longshore sand transport is a part of a much broader process termed here margin-parallel sediment transport (MPST). Sand is transported in a nearshore shallow water belt where marine currents are highly energetic. Shale transport occurs at

greater depths over the deeper shelf and the continental slope where marine currents are weaker.

2. Without the large transport of silt and clay in the deeper waters, deposition offshore Israel probably would have been negligible, and the Levant shelf never would have developed.
3. The delay in the formation of the Levant continental shelf relative to the Nile Delta is not a result of external forcing. MPST has begun coevally with delta formation but developed slower. Initially, a continental shelf formed offshore Sinai, then offshore Israel, and most recently along the Lebanese coast.
4. Throughout this time, longshore sand transport and deposition has taken place very close to the coastline, but only recently (last hundreds of thousands or tens of thousands of years), when the shelf became shallow enough, sand transport and deposition expanded 10-20 km westwards. This implies subaerial exposure of sandy landscape during recent eustatically low stands.
5. Down slope sediment transport into deep basins is relatively energetic and carries sand, silt, and clay, whereas margin-parallel currents are relatively weak and carry mainly silt and clay. One exception within the margin-parallel system is the highly energetic nearshore current that transport sand. Thus, MPST is an efficient differentiator between shale and sand.

ACKNOWLEDGMENTS

This study was supported by the Israeli Ministry of Energy and by the Mediterranean Research Center of Israel (MERCI). The article is further based upon work of COST Action

“Uncovering the Mediterranean salt giant” (MEDSALT) supported by the European Cooperation in Science and Technology.

REFERENCES

Aal, A.A., El Barkooky, A., Gerrits, M., Meyer, H., Schwander, M., Zaki, H., 2000. Tectonic evolution of the Eastern Mediterranean Basin and its significance for hydrocarbon prospectivity in the ultradeepwater of the Nile Delta. Lead. Edge 19, 1086–1102. https://doi.org/10.1190/1.1438485

Adams, E.W., Schlager, W., Wattel, E., 1998. Submarine slopes with an exponential curvature. Sediment. Geol. 117, 135–141.

Almogi-Labin, A., Calvo, R., Elyashiv, H., Amit, R., Harlavan, Y., Herut, B., 2012. Sediment characterization of the Israeli Mediterranean shelf (10-100 m).

Amadori, C., Garcia-Castellanos, D., Toscani, G., Sternai, P., Fantoni, R., Ghielmi, M., Di Giulio, A., 2018. Restored topography of the Po Plain-Northern Adriatic region during the Messinian base-level drop—Implications for the physiography and compartmentalization of the palaeo-Mediterranean basin. Basin Res. 30, 1247–1263.

Amante, C., Eakins, B.W., 2009. ETOPO1 arc-minute global relief model: procedures, data sources and analysis.

Amit, R., Enzel, Y., Crouvi, O., Simhai, O., Matmon, A., Porat, N., McDonald, E., Gillespie, A.R., 2011. The role of the Nile in initiating a massive dust influx to the Negev late in the middle Pleistocene. Geol. Soc. Am. Bull. 123, 873–889. https://doi.org/10.1130/B30241.1

Bar, O., 2009. The shaping of the continental margin of central Israel since the Late Eocene—Tectonics, morphology and stratigraphy. Geol. Surv. Isr. Rep. GSI/32/2009.

Bar, O., Gvirtzman, Z., Feinstein, S., Zilberman, E., 2013. Accelerated subsidence and sedimentation in the levant basin during the late tertiary and concurrent uplift of the arabian platform: Tectonic versus counteracting sedimentary loading effects. Tectonics 32, 334–350. https://doi.org/10.1002/tect.20026

Barber, P.M., 1981. Messinian subaerial erosion of the proto-Nile Delta. Mar. Geol. 44, 253–272. https://doi.org/10.1016/0025-3227(81)90053-0

Begin, Z.B., Meyer, D.F., Schumm, S.A., 1981. Development of longitudinal profiles of alluvial channels in response to base-level lowering. Earth Surf. Process. Landforms 6, 49–68. https://doi.org/10.1002/esp.3290060106

Ben-Avraham, Z., 1978. The structure and tectonic setting of the levant continental margin, Eastern Mediterranean. Tectonophysics 46, 313–331. https://doi.org/10.1016/0040-1951(78)90210-X

Ben-Gai, Y., Ben-Avraham, Z., Buchbinder, B., Kendall, C.G.S.C., 2005. Post-Messinian evolution of the Southeastern Levant Basin based on two-dimensional stratigraphic simulation. Mar. Geol. 221, 359–379. https://doi.org/10.1016/j.margeo.2005.03.003

Ben-Zeev, Y., Gvirtzman, Z., 2019. When two Salt Tectonic systems meet: gliding downslope the Levant Margin and salt-squeezing from under the Nile Delta. The Hebrew University of Jerusalem.

Ben Moshe, L., Haviv, I., Enzel, Y., Zilberman, E., Matmon, A., 2008. Incision of alluvial channels in response to a continuous base level fall: Field characterization, modeling, and validation along the Dead Sea. Geomorphology 93, 524–536. https://doi.org/10.1016/J.GEOMORPH.2007.03.014

Ben Zeev, Y., Gvirtzman, Z., 2020. WHEN TWO SALT TECTONICS SYSTEMS MEET: GLIDING

DOWNSLOPE THE LEVANT MARGIN AND SALT OUT-SQUEEZING FROM UNDER THE NILE DELTA. Tectonics e2019TC005715.

Buchbinder, B., Gvirtzman, G., 1976. The break-up of the Tethys Ocean into the Mediterranean Sea, the Red Sea, and the Mesopotamian Basin during the Miocene: a sequence of fault movements and desiccation events, in: Abstract of the Fi Rst Congress Pacifi c Neog. Stratigr. pp. 32–35.

Buchbinder, B., Martinotti, G.M., Siman-Tov, R., Zilberman, E., 1993. Temporal and spatial relationships in Miocene reef carbonates in Israel. Palaeogeogr. Palaeoclimatol. Palaeoecol. 101, 97–116. https://doi.org/10.1016/0031-0182(93)90154-B

Buchbinder, B., Zilberman, E., 1997. Sequence stratigraphy of Miocene-Pliocene carbonate-siliciclastic shelf deposits in the eastern Mediterranean margin (Israel): effects of eustasy and tectonics. Sediment. Geol. 112, 7–32. https://doi.org/10.1016/S0037-0738(97)00034-1

Carmel, Z., Inman, D.L., Golik, A., 1985. Directional wave measurement at Haifa, Israel, and sediment transport along the Nile littoral cell. Coast. Eng. 9, 21–36. https://doi.org/10.1016/0378-3839(85)90025-0

Coulthard, T.J., 1999. Modelling upland catchment response to Holocene environmental change.

Crouvi, O., Amit, R., Enzel, Y., Porat, N., Sandler, A., 2008. Sand dunes as a major proximal dust source for late Pleistocene loess in the Negev Desert, Israel. Quat. Res. 70, 275–282. https://doi.org/10.1016/j.yqres.2008.04.011

Csato, I., Catuneanu, O., Granjeon, D., 2014. Millennial-Scale Sequence Stratigraphy: Numerical Simulation With Dionisos. J. Sediment. Res. 84, 394–406.

https://doi.org/10.2110/jsr.2014.36

Csato, I., Granjeon, D., Catuneanu, O., Baum, G.R., 2013. A three-dimensional stratigraphic model for the Messinian crisis in the Pannonian Basin, eastern Hungary. Basin Res. 25, 121–148. https://doi.org/10.1111/j.1365-2117.2012.00553.x

Culling, W.E.H., 1960. Analytical Theory of Erosion. J. Geol. 68, 336–344. https://doi.org/10.1086/626663

Dai, A., Trenberth, K.E., 2002. Estimates of freshwater discharge from continents: Latitudinal and seasonal variations. J. Hydrometeorol. 3, 660–687.

Davis, M., Matmon, A., Rood, D.H., Avnaim-Katav, S., 2012. Constant cosmogenic nuclide concentrations in sand supplied from the Nile River over the past 2.5 m.y. Geology 40, 359–362. https://doi.org/10.1130/G32574.1

Deville, E., Mascle, A., Callec, Y., Huyghe, P., Lallemant, S., Lerat, O., Mathieu, X., Padron De Carillo, C., Patriat, M., Pichot, T., Loubrieux, B., Granjeon, D., 2015. Tectonics and sedimentation interactions in the east Caribbean subduction zone: An overview from the Orinoco delta and the Barbados accretionary prism. Mar. Pet. Geol. 64, 76–103. https://doi.org/10.1016/j.marpetgeo.2014.12.015

Druckman, Y., Buchbinder, B., Martinotti, G.M., Siman Tov, R., Aharon, P., 1995. The buried Afiq Canyon (eastern Mediterranean, Israel): a case study of a Tertiary submarine canyon exposed in Late Messinian times. Mar. Geol. 123, 167–185. https://doi.org/10.1016/0025-3227(94)00127-7

El Din, S.H.S., Mahar, A.M., 1997. Evaluation of sediment transport along the Nile Delta coast, Egypt. J. Coast. Res. 23–26.

Elfassi, Y., Gvirtzman, Z., Katz, O., Aharonov, E., 2019. Chronology of post-Messinian faulting

along the Levant continental margin and its implications for salt tectonics. Mar. Pet. Geol. 109, 574–588. https://doi.org/10.1016/J.MARPETGEO.2019.05.032

Emery, K.O., Bentor, Y.K., 1960. The continental shelf of Israel. State of Israel, Ministry of Development, Geological Survey.

Emery, K.O., Neev, D., Bentor, Y.K., 1960. Mediterranean beaches of Israel. State of Israel, Ministry of Agriculture, Division of Fisheries, the Sea ….

Frey-Martınez, J., Hall, B., Cartwright, J., Huuse, M., 2007. Clastic Intrusion at the Base of Deep-water Sands: A Trap-forming Mechanism in the Eastern Mediterranean. Am. Assoc. Pet. Geol. 49–63. https://doi.org/10.1306/1209849M873255

Frey Martinez, J., Cartwright, J., Hall, B., 2005. 3D seismic interpretation of slump complexes: examples from the continental margin of Israel. Basin Res. 17, 83–108. https://doi.org/10.1111/j.1365-2117.2005.00255.x

Galloway, W.E., 1998. Siliciclastic slope and base-of-slope depositional systems: component facies, stratigraphic architecture, and classification. Am. Assoc. Pet. Geol. Bull. 82, 569–595.

Garcia-Castellanos, D., Vergés, J., Gaspar-Escribano, J., Cloetingh, S., 2003. Interplay between tectonics, climate, and fluvial transport during the Cenozoic evolution of the Ebro Basin (NE Iberia). J. Geophys. Res. Solid Earth 108. https://doi.org/10.1029/2002JB002073

Gardosh, M.A., Druckman, Y., Buchbinder, B., 2009. The Late Tertiary Deep-Water Siliciclastic System of the Levant Margin–An Emerging Play Offshore Israel. Am. Assoc. Pet. Geol. Search Discov. Artic. 10211.

Gerber, T.P., Amblas, D., Wolinsky, M.A., Pratson, L.F., Canals, M., 2009. A model for the long-

profile shape of submarine canyons. J. Geophys. Res. 114, F03002. https://doi.org/10.1029/2008JF001190

Goldsmith, V., Golik, A., 1980. Sediment transport model of the southeastern Mediterranean coast. Mar. Geol. 37, 147–175. https://doi.org/10.1016/0025-3227(80)90015-8

Golik, A., 2002. Pattern of sand transport along the Israeli coastline. Isr. J. Earth Sci. 51.

Golik, A., 1997. Dynamics and management of sand along the Israeli coastline. Bull. Oceanogr. MONACO-NUMERO Spec. 97–110.

Golik, A., 1993. Indirect evidence for sediment transport on the continental shelf off Israel. Geo-Marine Lett. 13, 159–164. https://doi.org/10.1007/BF01593189

Golik, A., Rosen, D.S., Brachia, V., 1999. Management of the Israeli coastal sand resources. CAMPIsrael, Mediterr. Action Plan, UNEP Isr. Minist. Environ. IOLR ReportH28/1999, Haifa).

Granjeon, D., 2014. 3D forward modelling of the impact of sediment transport and base level cycles on continental margins and incised valleys, in: From Depositional Systems to Sedimentary Successions on the Norwegian Continental Margin. John Wiley & Sons, Ltd, Chichester, UK, pp. 453–472. https://doi.org/10.1002/9781118920435.ch16

Granjeon, D., 2009. 3D stratigraphic modeling of sedimentary basins. AAPG Search Discov. Artic.

Granjeon, D., 1997. Modélisation stratigraphique déterministe: Conception et application d'un modèle diffusif 3D multilithologique. Univ. of Rennes.

Granjeon, D., Joseph, P., 1999. Concepts and applications of a 3-D multiple lithology, diffusive model in stratigraphic modeling.

Granjeon, D., Wolf, S., 2007. 3D stratigraphic modeling in complex tectonics area, in:

Abstract of the AAPG Annual Convention and Exhibition. AAPG Search and Discovery Long Beach, California, USA.

Gvirtzman, G., 1970. The Saqiye Group in the coastal plain and Hashfela regions, Israel, Isr. Geol. Surv., Rep. OD'S.

Gvirtzman, G., Buchbinder, B., 1978. The Late Tertiary of the coastal plain and continental shelf of Israel and its bearing on the history of the Eastern Mediterranean, Initial reports of the deep sea drilling project.

Gvirtzman, G., Buchbinder, B., 1969. Outcrops of Neogene Formation in the Central and Southern Coastal Plain, Hashephela and Beer Sheva'Regions, Israel. Geological Survey.

Gvirtzman, Z., Csato, I., Granjeon, D., 2014. Constraining sediment transport to deep marine basins through submarine channels : The Levant margin in the Late Cenozoic. Mar. Geol. 347, 12–26.

Haq, B., Hardenbohl, J., Vail, P.R., 1987. Chronology of fluctuating sea levels since the Triasic (250 million years ago to present). Sci. York.

Harel, M., Amit, R., Porat, N., Enzel, Y., 2016. Evolution in of the southeastern Mediterranean coastal plain, in: Quaternary of the Levant: Environments, Climate Change, and Humans. Cambridge University Press Cambridge.

Harris, A.D., Covault, J.A., Madof, A.S., Sun, T., Sylvester, Z., Granjeon, D., 2016. Three-Dimensional Numerical Modeling of Eustatic Control On Continental-Margin Sand Distribution. J. Sediment. Res. 86, 1434–1443. https://doi.org/10.2110/jsr.2016.85

Hawie, N., Barrois, A., Marfisi, E., Murat, B., Hall, J., El-Wazir, Z., Al-Madani, N., Aillud, G., 2015. Forward Stratigraphic Modelling, Deterministic Approach to Improve Carbonate Heterogeneity Prediction; Lower Cretaceous, Abu Dhabi, in: Abu Dhabi International

Petroleum Exhibition and Conference. Society of Petroleum Engineers. https://doi.org/10.2118/177519-MS

Hawie, N., Covault, J.A., Dunlap, D., Sylvester, Z., 2018. Slope-fan depositional architecture from high-resolution forward stratigraphic models. Mar. Pet. Geol. 91, 576–585. https://doi.org/10.1016/J.MARPETGEO.2017.12.033

Hawie, N., Deschamps, R., Granjeon, D., Nader, F.H., Gorini, C., Müller, C., Montadert, L., Baudin, F., 2017. Multi-scale constraints of sediment source to sink systems in frontier basins: a forward stratigraphic modelling case study of the Levant region. Basin Res. 29, 418–445. https://doi.org/10.1111/bre.12156

Hsü, K.J., Ryan, W.B.F., Cita, M.B., 1973. Late Miocene dessication of the Mediterranean. Nature 242, 240–244.

Inman, D.L., Brush, B.M., 1973. The coastal challenge. Science (80-.). 181, 20–32. https://doi.org/10.1126/science.181.4094.20

Inman, D.L., Elwany, M.H.S., Khafagy, A.A., Golik, A., 1993. Nile Delta profiles and migrating sand blankets, in: Coastal Engineering 1992. pp. 3273–3284.

Inman, D.L., Jenkins, S.A., 1984. The Nile littoral cell and man's impact on the coastal littoral zone in the SE Mediterranean, in: Proceedings of the 17th International Coastal Engineering Conference. ASCE Sydney, Australia, pp. 1600–1617.

Inman, D.L., Nordstrom, C.E., Flick, R.E., 1976. Currents in submarine canyons: An air-sea-land interaction. Annu. Rev. Fluid Mech. 8, 275–310.

Jordan, T.E., Flemings, P.B., 1991. Large-scale stratigraphic architecture, eustatic variation, and unsteady tectonism: A theoretical evaluation. J. Geophys. Res. Solid Earth 96, 6681–6699. https://doi.org/10.1029/90JB01399@10.1002/(ISSN)2169-

9356.LTSLC1

Kaufman, P., Grotzinger, J., McCormick, D., 1991. Depth-dependent diffusion algorithm for simulation of sedimentation in shallow marine deposition systems. Sediment. Model. Camputer Simulations Methods Improv. Param. Defin.

Kellner, A., Khawaga, H. El, Brink, G., Brink-larsen, S., Hesham, M., Abu, H., Saad, E., Atef, A., Young, H., Finlayson, B., 2009. Depositional History of the West Nile Delta – Upper Oligocene to Upper Pliocene, in: AAPG International Conference and Exhibition, Cape Town, South Africa.

Kempler, D., 1998. Eratosthenes Seamount: The possible spearhead of incipient continental collision in the eastern Mediterranean. Proc. Ocean Drill. Progr. Sci. Results 160, 709–722. https://doi.org/10.2973/odp.proc.sr.160.031.1998

Kenyon, P.M., Turcotte, D.L., 1985. Morphology of a delta prograding by bulk sediment transport. Geol. Soc. Am. Bull. 96, 1457. https://doi.org/10.1130/0016-7606(1985)96<1457:MOADPB>2.0.CO;2

Klein, M., Zviely, D., Kit, E., Shteinman, B., 2007. Sediment transport along the coast of Israel: examination of fluorescent sand tracers. J. Coast. Res. 1462–1470.

Lai, S.Y.J., Capart, H., 2007. Two-diffusion description of hyperpycnal deltas. J. Geophys. Res. 112, F03005. https://doi.org/10.1029/2006JF000617

Laurent, D., Marsset, T., Droz, L., Granjeon, D., Molliex, S., Picot, M., Rabineau, M., 2020. 4D forward stratigraphic modelling of the Late Quaternary Congo deep-sea fan: Role of climate/vegetation coupling in architectural evolution. Mar. Geol. 429, 106334.

Manohar, M., 1981. Coastal processes at the Nile Delta coast. SHORE & BEACH 49, 8–15.

Milliman, J.D., Syvitski, J.P.M., 1992. Geomorphic/Tectonic Control of Sediment Discharge to

the Ocean: The Importance of Small Mountainous Rivers. J. Geol. 100, 525–544. https://doi.org/10.1086/629606

Mitchell, N.C., Huthnance, J.M., 2008. Oceanographic Currents and the Convexity of the Uppermost Continental Slope. J. Sediment. Res. 78, 29–44. https://doi.org/10.2110/jsr.2008.006

Mitchell, N.C., Huthnance, J.M., 2007. Comparing the smooth, parabolic shapes of interfluves in continental slopes to predictions of diffusion transport models. Mar. Geol. 236, 189–208. https://doi.org/10.1016/J.MARGEO.2006.10.028

Murray, A.B., Paola, C., 1994. A cellular model of braided rivers. Nature 371, 54.

Nachmias, J., 1969. Source rocks of the Saqiye Group sediments in the coastal plain of Israel—a heavy mineral study. Isr. J. Earth-Sciences 18, 1–16.

Paola, C., Heller, P.L., Angevine, C.L., 1992. The large-scale dynamics of grain-size variation in alluvial basins, 1: Theory. Basin Res. 4, 73–90.

Parker, G., Paola, C., Whipple, K.X., Mohrig, D., 1998. Alluvial fans formed by channelized fluvial and sheet flow. I: Theory. J. Hydraul. Eng. 124, 985–995.

Perlin, A., Kit, E., 1999. Longshore sediment transport on Mediterranean coast of Israel. J. Waterw. Port, Coastal, Ocean Eng. 125, 80–87.

Rabineau, M., Berné, S., Aslanian, D., Olivet, J.L., Joseph, P., Guillocheau, F., Bourillet, J.F., Ledrezen, E., Granjeon, D., 2005. Sedimentary sequences in the Gulf of Lion: a record of 100,000 years climatic cycles. Mar. Pet. Geol. 22, 775–804.

Rabineau, M., Berné, S., Olivet, J.-L., Aslanian, D., Guillocheau, F., Joseph, P., 2006. Paleo sea levels reconsidered from direct observation of paleoshoreline position during Glacial Maxima (for the last 500,000 yr). Earth Planet. Sci. Lett. 252, 119–137.

Rebesco, M., 2018. Sedimentary Environments: Contourites. Ref. Modul. Earth Syst. Environ. Sci. https://doi.org/10.1016/B978-0-12-409548-9.09094-1

Rebesco, M., 2005. SEDIMENTARY ENVIRONMENTS | Contourites. Encycl. Geol. 513–527. https://doi.org/10.1016/B0-12-369396-9/00497-4

Rebesco, M., Camerlenghi, A., 2008. Contourites. Elsevier.

Rebesco, M., Hernández-Molina, F.J., Van Rooij, D., Wåhlin, A., 2014. Contourites and associated sediments controlled by deep-water circulation processes: State-of-the-art and future considerations. Mar. Geol. 352, 111–154. https://doi.org/10.1016/J.MARGEO.2014.03.011

Rivenæs, J.C., 1997. Impact of sediment transport efficiency on large-scale sequence architecture: results from stratigraphic computer simulation. Basin Res. 9, 91–105. https://doi.org/10.1046/j.1365-2117.1997.00037.x

Robertson, A.H.F., 1998. Tectonic significance of the Eratosthenes Seamount: A continental fragment in the process of collision with a subduction zone in the eastern Mediterranean (Ocean Drilling Program Leg 160). Tectonophysics 298, 63–82. https://doi.org/10.1016/S0040-1951(98)00178-4

Rosentraub, Z., Brenner, S., 2007. Circulation over the southeastern continental shelf and slope of the Mediterranean Sea: Direct current measurements, winds, and numerical model simulations. J. Geophys. Res. 112, C11001. https://doi.org/10.1029/2006JC003775

Ryan, W.B.F., Cita, M.B., 1978. The nature and distribution of Messinian erosional surfaces — Indicators of a several-kilometer-deep Mediterranean in the Miocene. Mar. Geol. 27, 193–230. https://doi.org/10.1016/0025-3227(78)90032-4

Said, R., 1981. The Geological Evolution of the River Nile, The GEOLOGICAL EVOLUTION of the RIVER NILE. Springer Science & Business Media, New York, NY. https://doi.org/10.1007/978-1-4612-5841-4_1

Schattner, U., 2010. What triggered the early-to-mid Pleistocene tectonic transition across the entire eastern Mediterranean? Earth Planet. Sci. Lett. 289, 539–548. https://doi.org/10.1016/J.EPSL.2009.11.048

Schattner, U., Gurevich, M., Kanari, M., Lazar, M., 2015. Levant jet system-effect of post LGM seafloor currents on Nile sediment transport in the eastern Mediterranean. Sediment. Geol. 329, 28–39. https://doi.org/10.1016/j.sedgeo.2015.09.007

Schattner, U., Lazar, M., 2016. Hierarchy of source-to-sink systems — Example from the Nile distribution across the eastern Mediterranean. Sediment. Geol. 343, 119–131. https://doi.org/10.1016/j.sedgeo.2016.08.006

Schlager, W., Adams, E.W., 2001. Model for the sigmoidal curvature of submarine slopes. Geology 29, 883–886.

Sestini, G., 1989. Nile Delta: a review of depositional environments and geological history. Geol. Soc. London, Spec. Publ. 41, 99–127. https://doi.org/10.1144/GSL.SP.1989.041.01.09

Seymour, R.J., 2005. Longshore Sediment Transport. Encycl. Coast. Sci. 600.

Shoshany, M., Golik, A., Degani, A., Lavee, H., Gvirtzman, G., 1996. New evidence for sand transport direction along the coastline of Israel. J. Coast. Res. 311–325.

Shukri, N.M., 1950. The mineralogy of some Nile sediments. Q. J. Geol. Soc. 106, 466–467. https://doi.org/10.1144/GSL.JGS.1950.106.01-04.23

Shukri, N.M., Philip, G., 1960. The mineralogy of some recent deposits in the Arish-Gaza

area. Bull. Fac. Sci. Cairo Univ. 35, 73–85.

Spinewine, B., Sun, T., Babonneau, N., Parker, G., 2011. Self-similar long profiles of aggrading submarine leveed channels: Analytical solution and its application to the Amazon channel. J. Geophys. Res. 116, F03004. https://doi.org/10.1029/2010JF001937

Stanley, D.J., Warne, A.G., 1998. Nile Delta in Its Destruction Phase. J. Coast. Res. 14, 794–825.

Stanley, J.D., 1989. Sediment Transport on the Coast and Shelf Between the Nile Delta and Israeli Margin as Determined by Heavy Minerals. J. Coast. Res. 5, 813–828.

Steckler, M.S., Mountain, G.S., Miller, K.G., Christie-Blick, N., 1999. Reconstruction of Tertiary progradation and clinoform development on the New Jersey passive margin by 2-D backstripping. Mar. Geol. 154, 399–420. https://doi.org/10.1016/S0025-3227(98)00126-1

Syvitski, J.P.M., Milliman, J.D., 2007. Geology, geography, and humans battle for dominance over the delivery of fluvial sediment to the coastal ocean. J. Geol. 115, 1–19.

Tibor, G., Ben-Avraham, Z., Steckler, M., Fligelman, H., 1992. Late Tertiary subsidence history of the southern Levant Margin, eastern Mediterranean Sea, and its implications to the understanding of the Messinian Event. J. Geophys. Res. 97, 17593. https://doi.org/10.1029/92JB00978

Tucker, G.E., Slingerland, R.L., 1994. Erosional dynamics, flexural isostasy, and long-lived escarpments: A numerical modeling study. J. Geophys. Res. Solid Earth 99, 12229–12243. https://doi.org/10.1029/94JB00320

Van Heijst, M., Postma, G., Meijer, X.D., Snow, J.N., Anderson, J.B., 2001. Quantitative

analogue flume-model study of river-shelf systems: principles and verification exemplified by the Late Quaternary Colorado river-delta evolution. Basin Res. 13, 243–268.

Willgoose, G., Bras, R.L., Rodriguez-Iturbe, I., 1991. Results from a new model of river basin evolution. Earth Surf. Process. Landforms 16, 237–254. https://doi.org/10.1002/esp.3290160305

Woodward, J.C., Macklin, M.G., Krom, M.D., Williams, M.A.J., Gupta, A., 2007. The Nile: evolution, Quaternary river environments and material fluxes. Large rivers Geomorphol. Manag. 13, 712.

Young, A., Carson, M.A., Kirkby, M.J., 1973. Hillslope Form and Process. Geogr. J. 139, 140. https://doi.org/10.2307/1795822

Zaghloul, Z.M., El-Nasharty, F.A., Isa, I.A., 1982. Post-Aswan High Dam changes of the Nile Delta coast, east of Ras El Bar, interpreted from aerial photographs. Remote Sens. Arid semi-arid lands 877–883.

Zhang, J., Burgess, P.M., Granjeon, D., Steel, R., 2019. Can sediment supply variations create sequences? Insights from stratigraphic forward modelling. Basin Res. 31, 274–289. https://doi.org/10.1111/bre.12320

Zucker, E., Gvirtzman, Z., Steinberg, J., Enzel, Y., 2019. Salt tectonics in the Eastern Mediterranean Sea: Where a giant delta meets a salt giant. Geology. https://doi.org/10.1130/G47031.1

Zviely, D., Kit, E., Klein, M., 2007. Longshore sand transport estimates along the Mediterranean coast of Israel in the Holocene. Mar. Geol. 238, 61–73. https://doi.org/10.1016/J.MARGEO.2006.12.003

Zviely, D., Sivan, D., Ecker, A., Bakler, N., Rohrlich, V., Galili, E., Boaretto, E., Klein, M., Kit, E., 2006. Holocene evolution of the Haifa Bay area, Israel, and its influence on ancient tell settlements. The Holocene 16, 849–861.

FIGURE CAPTIONS

Figure 1: Topography and bathymetry map of the Eastern Mediterranean. Her = Herzliya. Ash = Ashkelon. ESM = Eratosthenes Seamount. Black circles mark oil and gas wells: 1=Mira, 2=Hannah 01, 3=Sara, 4=Hof Ashdod 01, 5=Yam 02, 6=Yinnon, 7=Maanit 01, 8=Caesarea. Black line w/triangles mark the Hellenic–Cyprus subduction. Dashed brown lines = Locations of cross sections. Black arrows – longshore sand transport (after Inman and Jenkins, 1984). Red arrows – LJS (after Schattner et al., 2015)

Figure 2: (A) Structural map of the base of the Pliocene. Black lines are faults after Aal et al. (2000). (B) A map showing the thickness of the Plio-Quaternary sedimentary sequence. Present-day coastline (gray line) is shown for reference. Figure after Zucker et al (2019).

Figure 3: (A) Reconstructed bathymetry for 5.3 Ma (obtained by flexural unloading of the PQ sediment from the base Pliocene map, see text). (B) Subsidence since the time of the base of the Pliocene sequence (5.3 Ma) until today. (C) 2D Illustration of the relationships between the data presented in Figs. 1-3.

Figure 4: (A) Sediment grain size as documented on the present-day seabed offshore Israel (after Almogi-Labin et al., 2012); the data indicate the coast-parallel distribution of the sand, silt, and clay belts. (B) Depth dependent sand/shale ratio parameters introduced in the model. Generated following Almogi-Labin et al. (2012).

Figure 5: Maps illustrating the evolution of the bathymetry through time as modeled by DionisosFlow using the basic sediment transport model without the MPST (see text). Red lines show locations of cross sections. (A) Same as Fig. 3A.

Figure 6: (A) Model results using a basic sediment transport that show a good fit with a cross section (B-B', see 6D for location) after Kellner et al. (2009) across the Nile Delta. (B) Cross section A-A' (see D for location) of the Nile Delta sand [%] that builds the delta at the end of the model that includes MPST (see text). (C) Interpreted seismic composite line across the Nile Delta (Kellner et al., 2009). (D) Location map of cross sections B-B', and A-A'. Dashed black line in cross section A-A', which shows present-day bathymetry. Color bar is the same for Figs. 6A and 6C.

Figure 7: (A and B) Results of chronostratigraphic model using basic sediment transport that indicate a bad fit to the observed present-day bathymetry reference (black dotted line) across the Levant continental margin. Black vertical lines mark locations of oil and gas wells with their names written above (see wells and cross section locations in Fig. 1).

Figure 8: (A) Total sediment thickness (from 5.3-0.0 Ma) as simulated without MPST (see text). (B) The difference in sequence thickness between simulated (A) and observed.

Figure 9: Bathymetry evolution through time as modeled by DionisosFlow implementing MPST. Note the difference between this model, which produces the Levant shelf, and the basic model that does not (Fig. 5). Red lines show locations of cross sections.

Figure 10: (A) Total sediment thickness, from 5.3 to 0.0 Ma generated by simulation including MPST (see text). (B) Difference between simulated (A) and observed sediment thickness. Note the relatively small difference here in comparison with the basic, without MPST, model (Fig. 8b).

Figure 11: (A and C) Chrono-stratigraphy of sections across the Levant margin derived from the model after adding the MPST. These sections show a good fit to observed sections based on seismic data (B and D). Black vertical lines in cross sections mark locations of oil and gas wells. Well names and cross section locations are in Fig. 1.

Figure 12: Simulated MPST cross sections (A and B) showing the resulted Kurkar (Mainly sand) and Yafo Formations (mainly shale); black rectangle in B shows the location of the enlarged cross section (C) (after Gvirtzman and Buchbinder, 1978). The sand fingers into the shaly section of Yafo Formation is the result of including the eustatic curve of Haq et al. (1987) in the model. (D) Location map. Color bar is the same for cross sections A and B.

Figure 13: The total sand thickness as simulated for the lower sequence (5.3-2.6 Ma) and for the upper sequence (2.6 -0.0 Ma), using the model without and with the MPST laws. (A) Lower sequence, using the basic model. (B) Lower sequence, using the MPST model. (C) Upper sequence, using the basic model. (D) Upper sequence, using the MPST model.

Figure 14: Sedimentation rates generated by both modeled scenarios in comparison with the observed sedimentation, divided into the four chronostratigraphic units determined by Ben Zeev and Gvirtzman (2020). White dotes mark the locations points taken, one in the deep basin and a second at the continental margin, for calculating sedimentation rates measured in figure 15.

Figure 15: Comparing sedimentation rates for the models without and MPST (red and gray, respectively) and the observed (black) sedimentation rate, divided in to two locations: Deep basin (solid line) and continental margin (dashed line). Locations in figure 14.

Figure 16: Sediment flux maps obtained by trial and error for lower (A) and upper (B) sequences printed over isobaths representing 3 Ma and 1 Ma, respectively. Each pixel in the

maps represents the flux (km^2My^{-1}) in a coast-parallel direction. Total sediment (D) and sand (C) fluxes crossing margin-perpendicular transects during deposition of lower and upper sequences. Curve representing the observed sand flux is based on references listed in the introduction.

Table 1: Model parameters from the literature and this study.

Figure 2

Click here to access/download;Figure;Fig 2.PNG

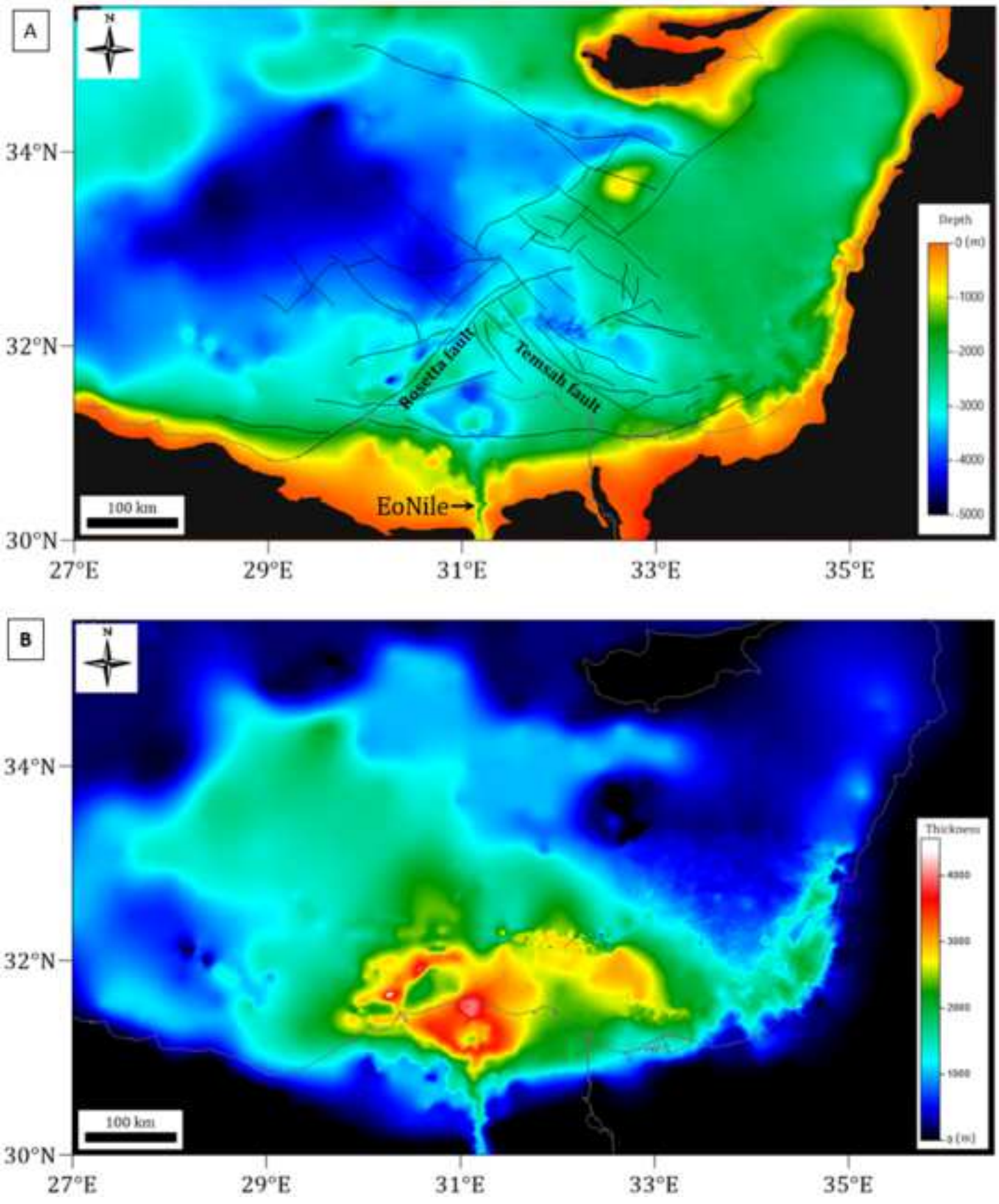

Figure 3

Click here to access/download;Figure;Fig 3.PNG

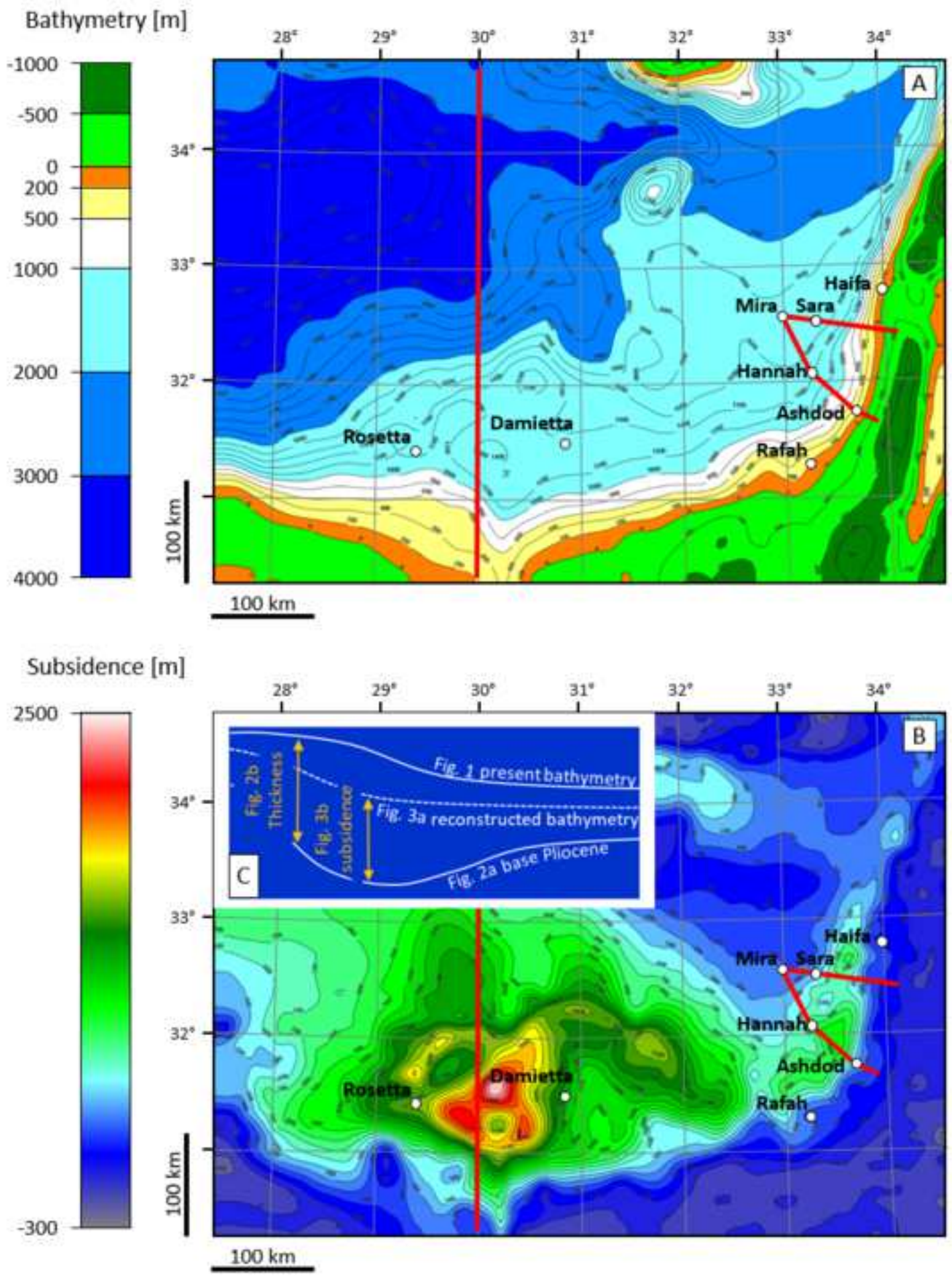

Figure 4

Click here to access/download;Figure;Fig 4.PNG

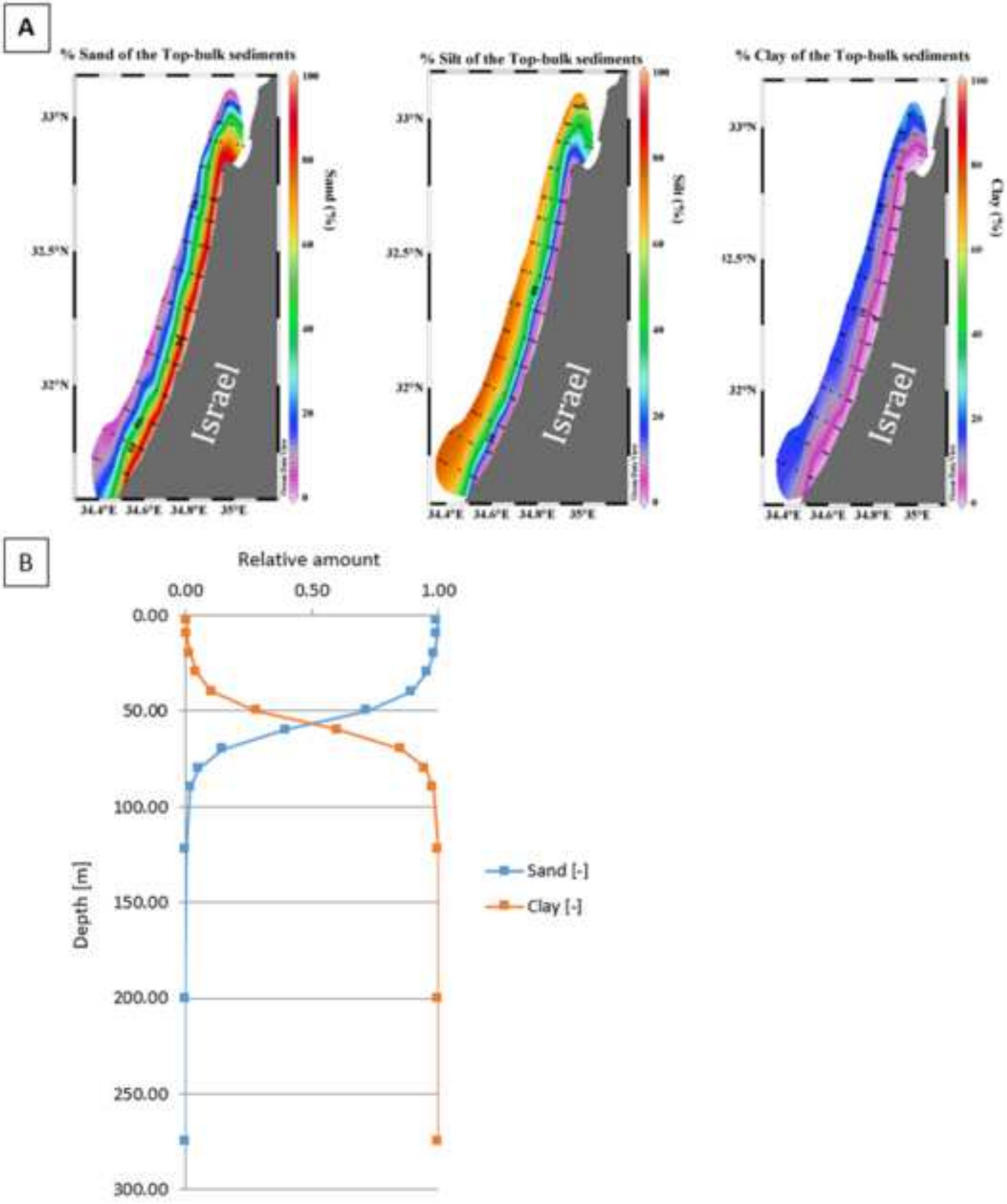

Figure 7

Click here to access/download;Figure;Fig 7.PNG

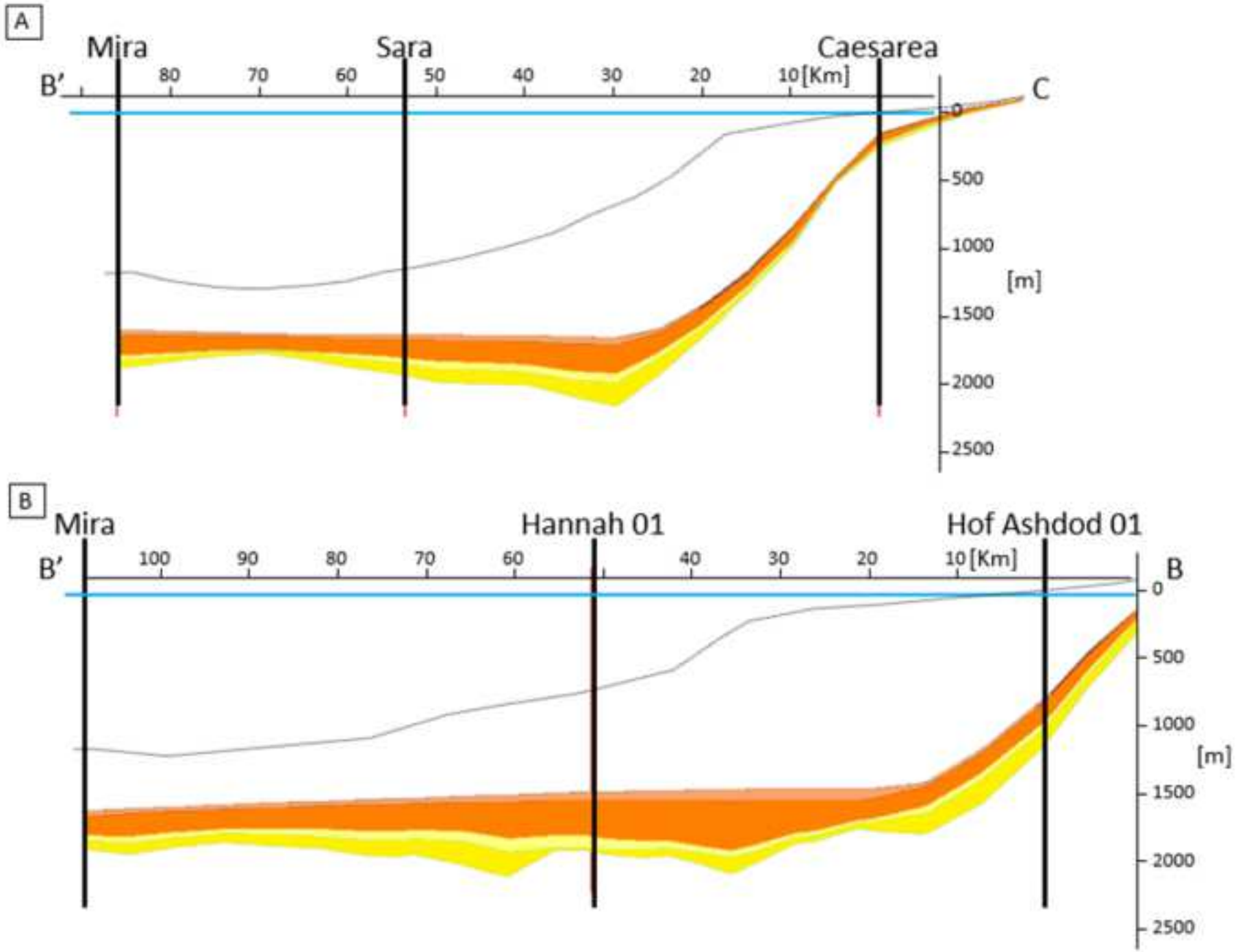

Figure 8

Click here to access/download;Figure;Fig 8.PNG

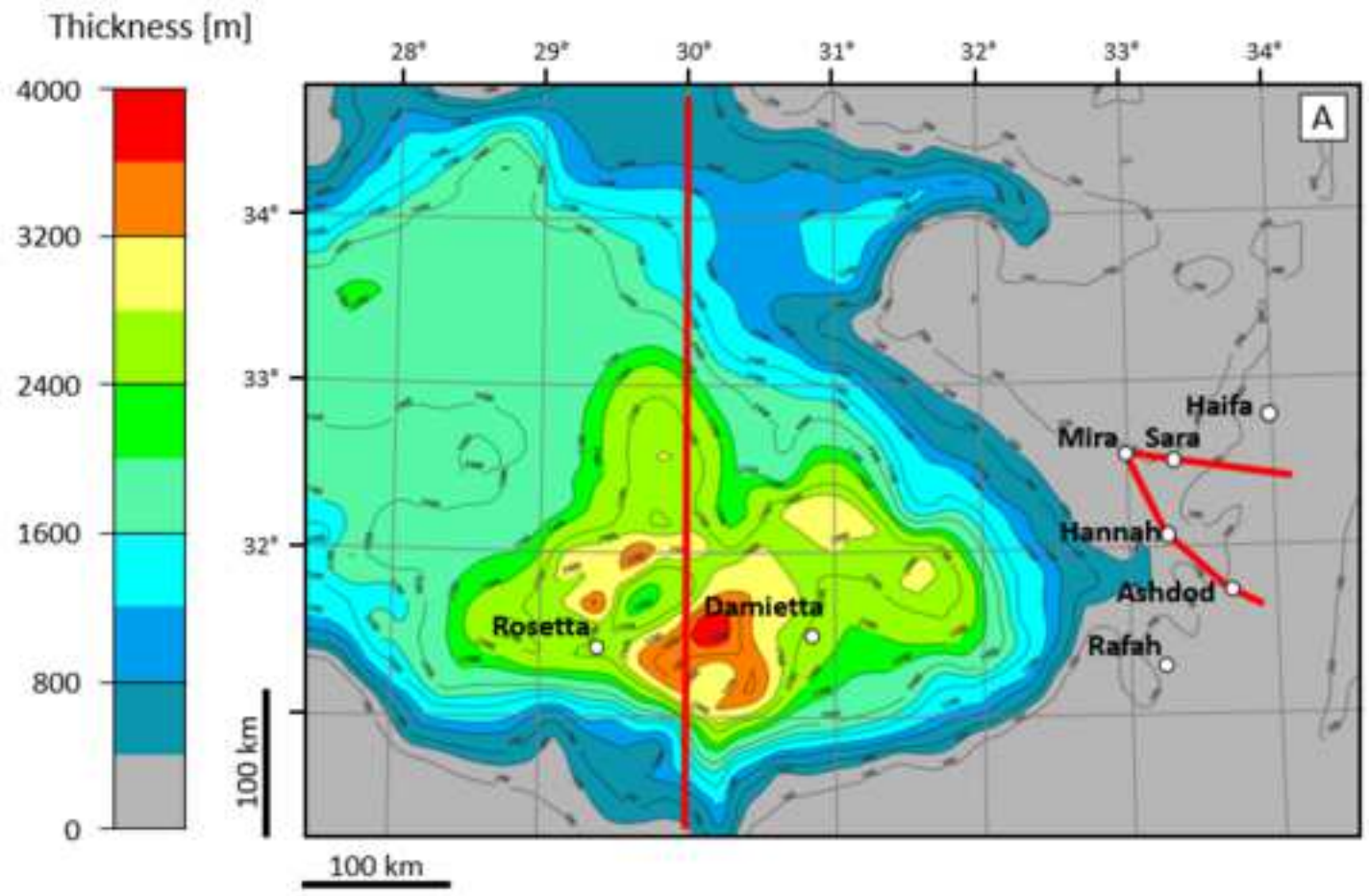

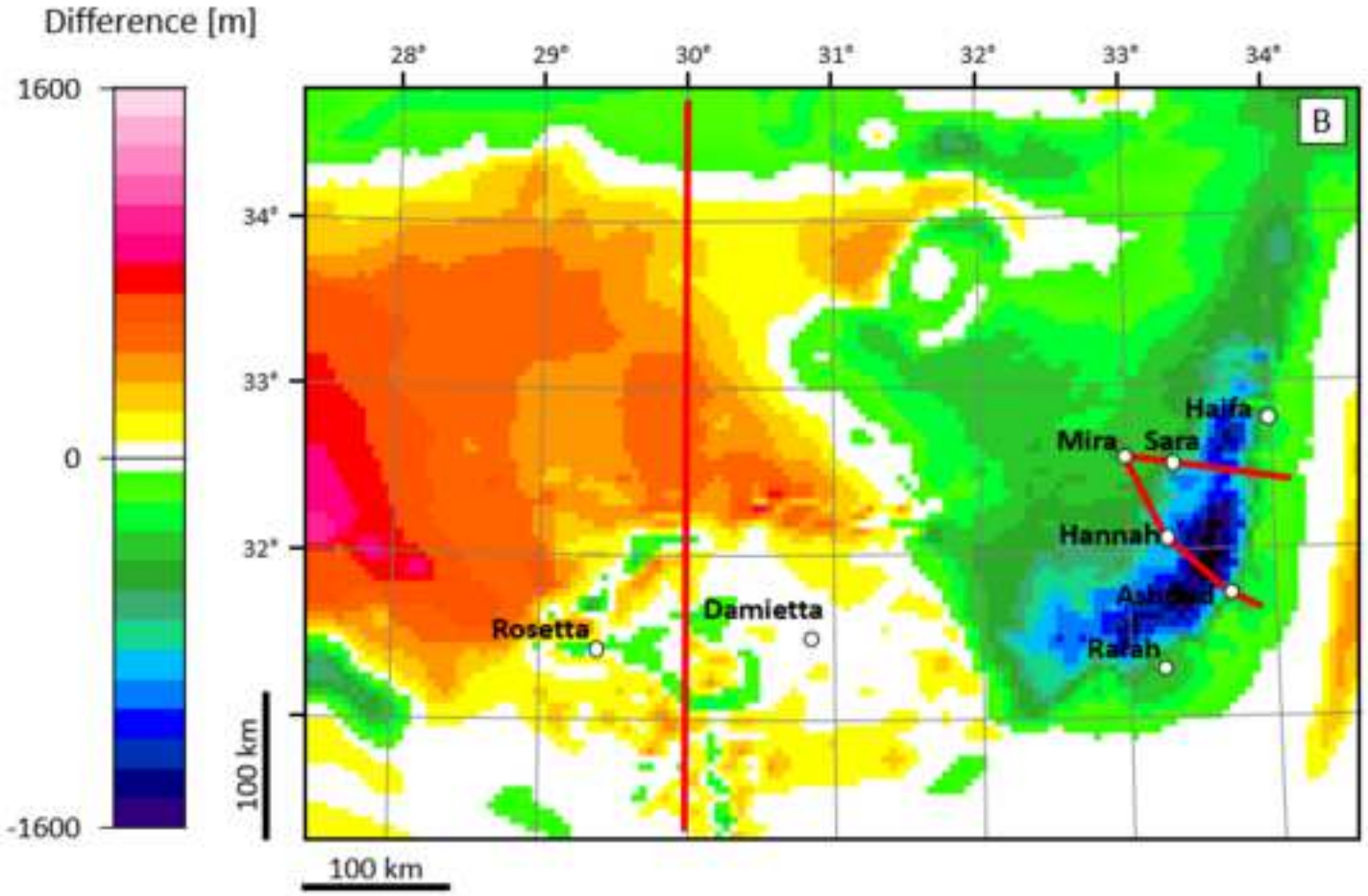

Figure 10

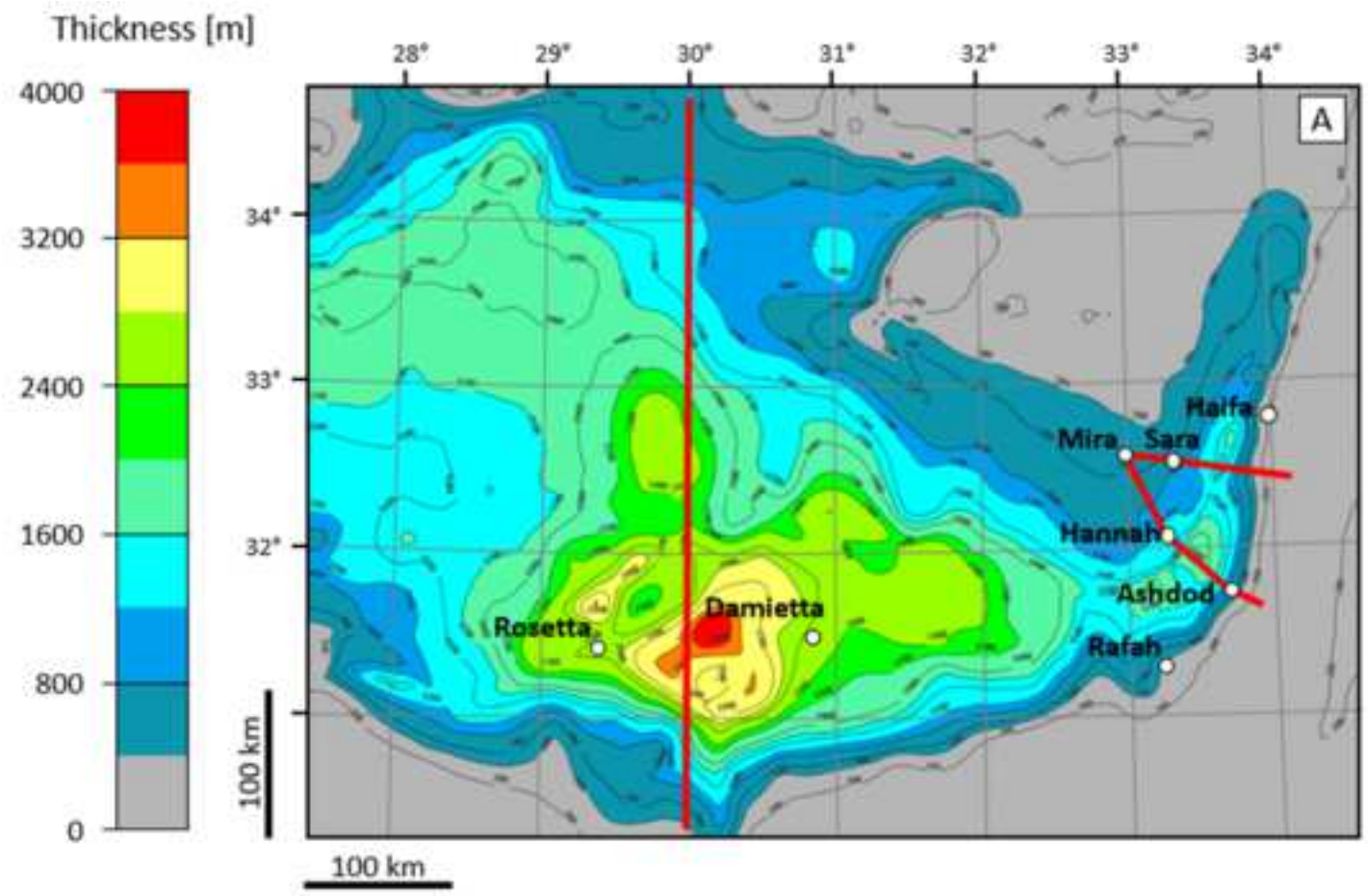

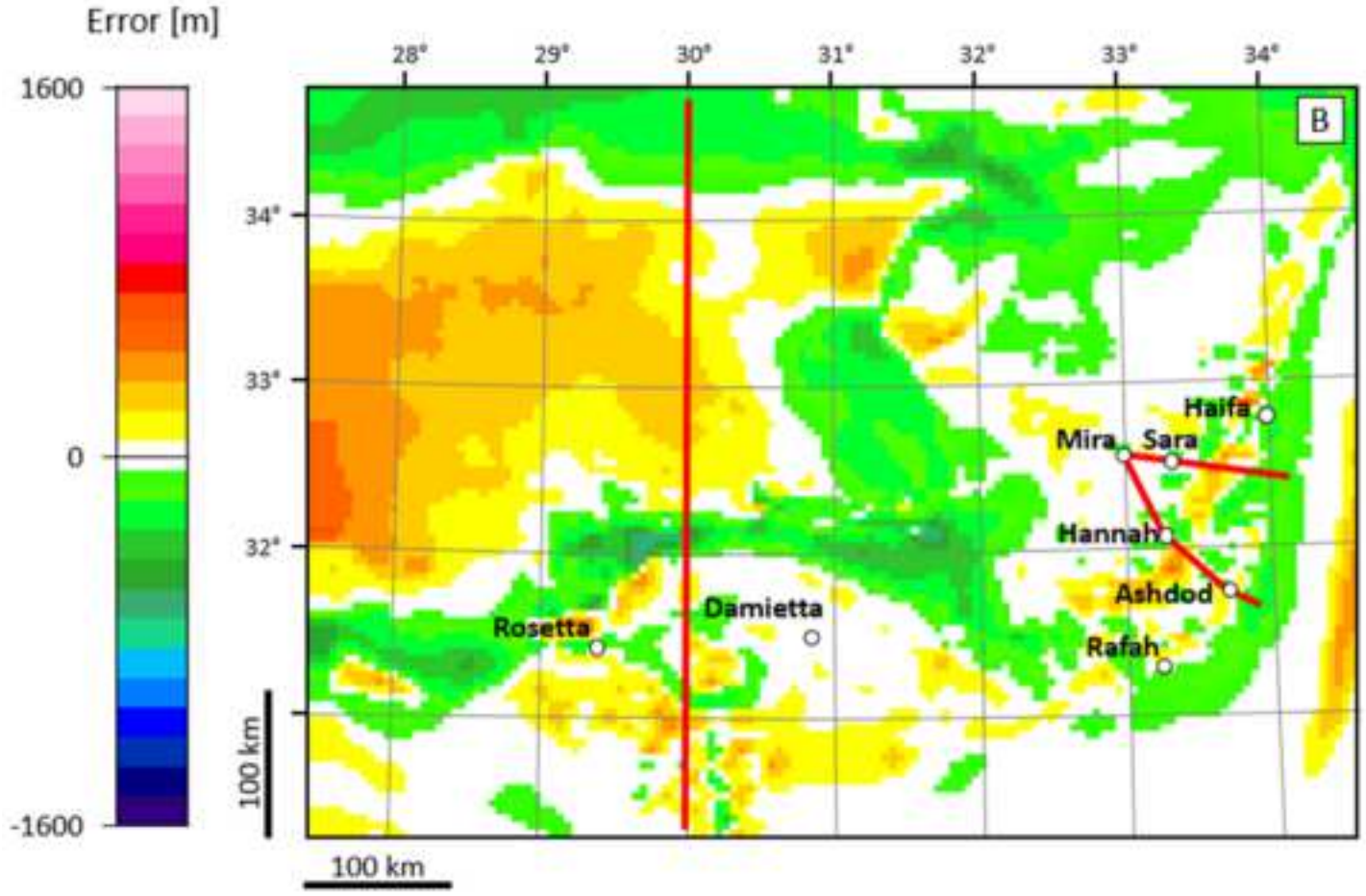

Figure 11

Click here to access/download;Figure;Fig 11.PNG

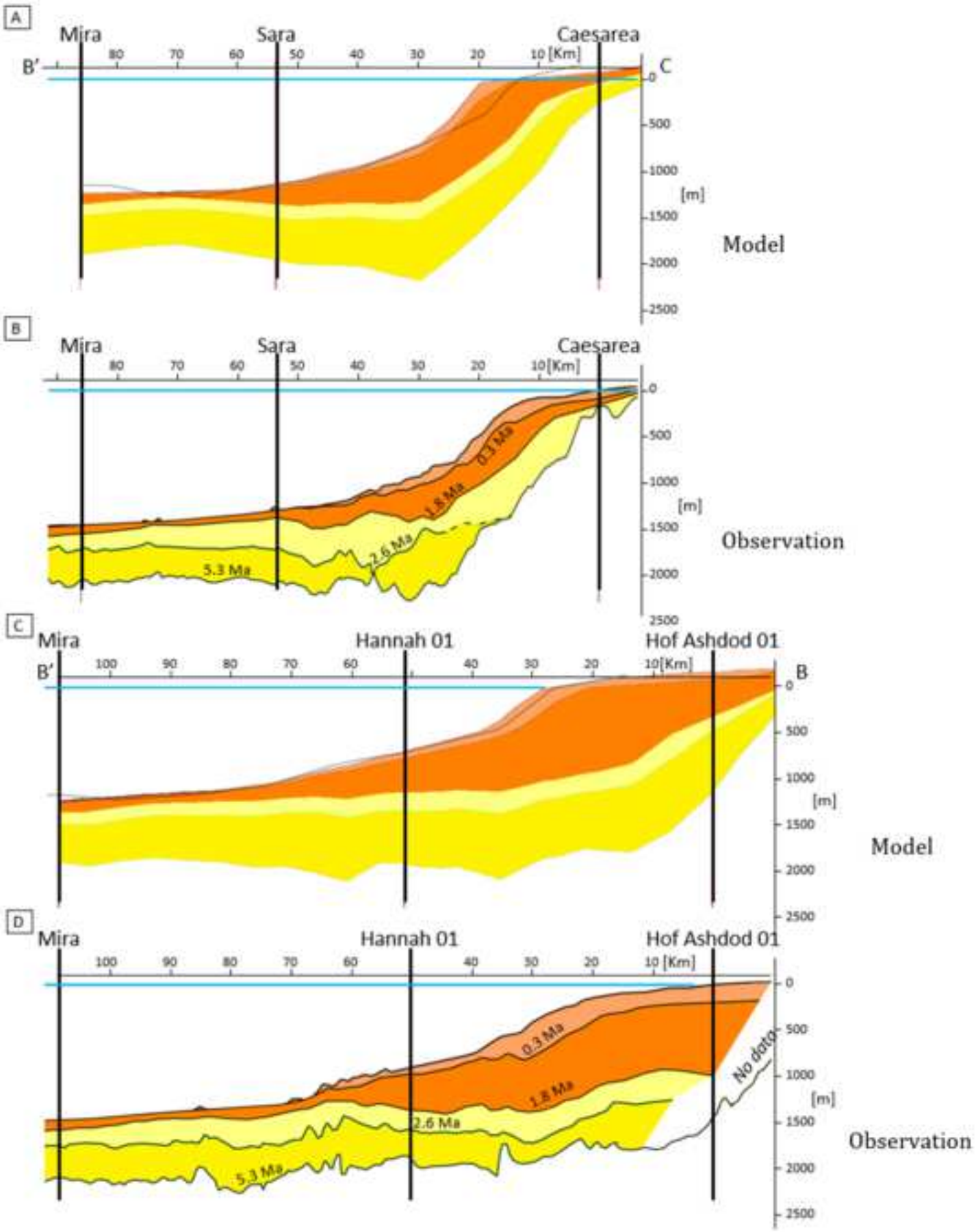

Figure 12

Click here to access/download;Figure;Fig 12.PNG

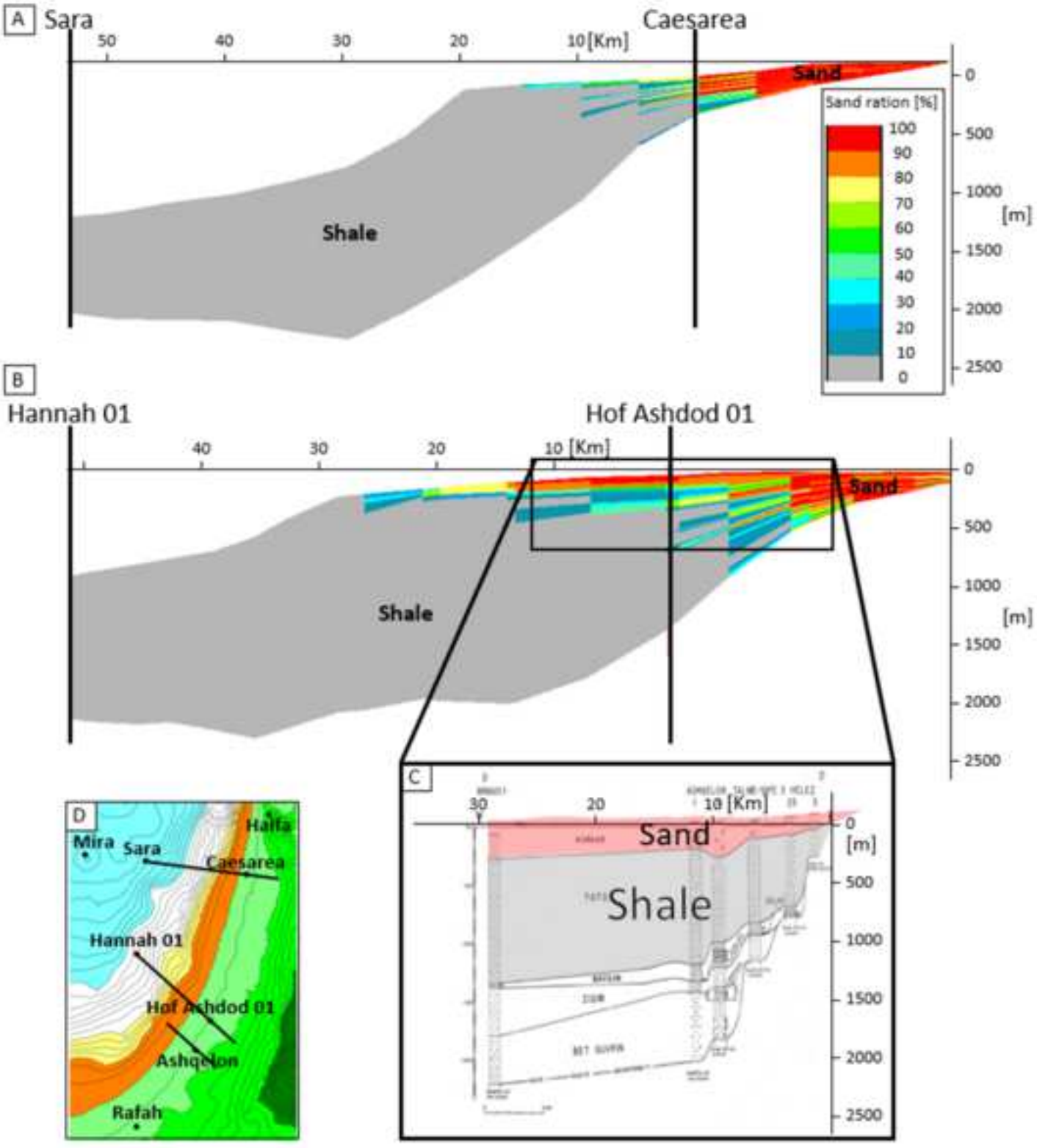

Figure 14

Click here to access/download;Figure;Fig 14.PNG

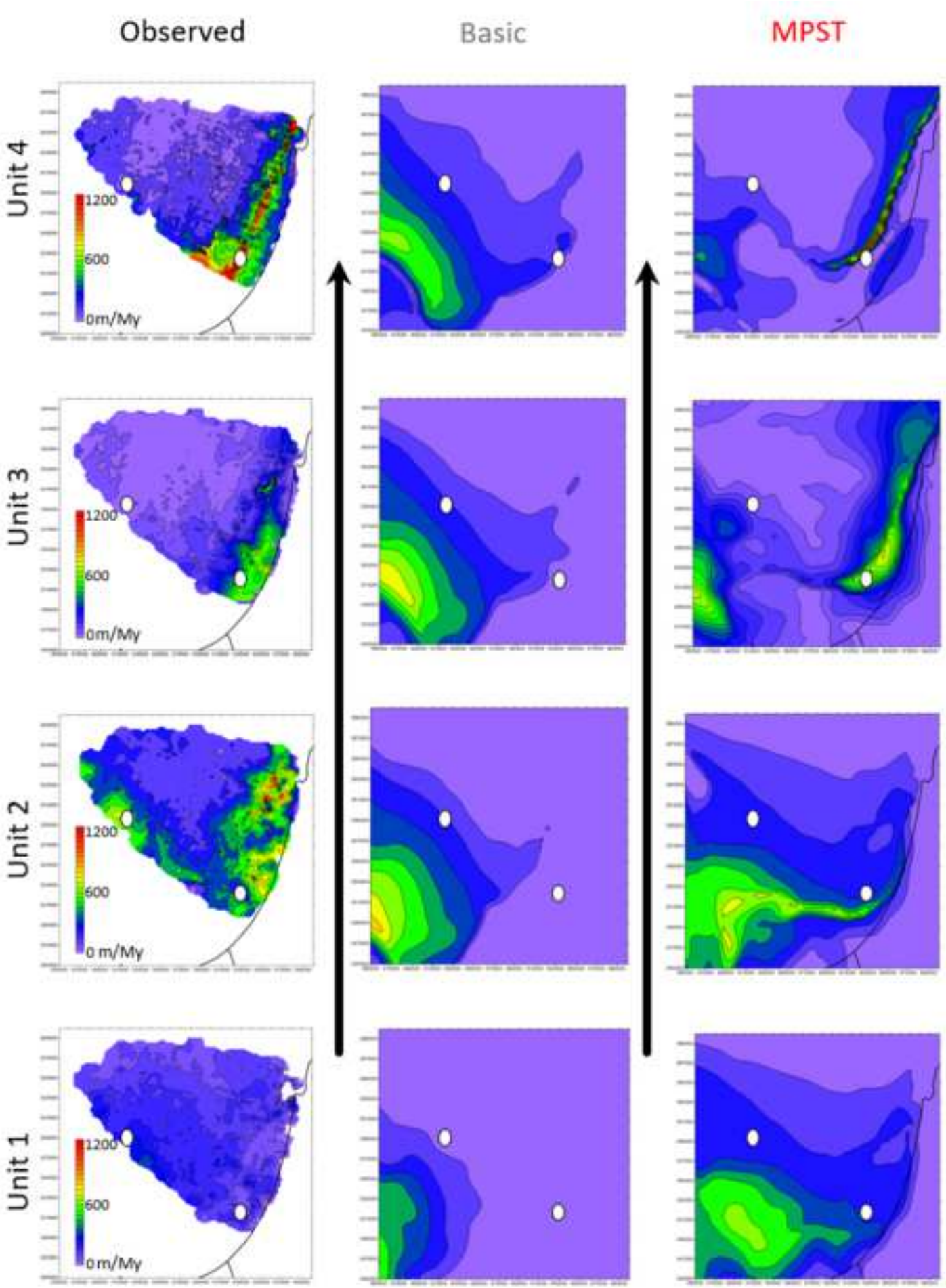

Figure 15

Click here to access/download;Figure;Fig 15.PNG

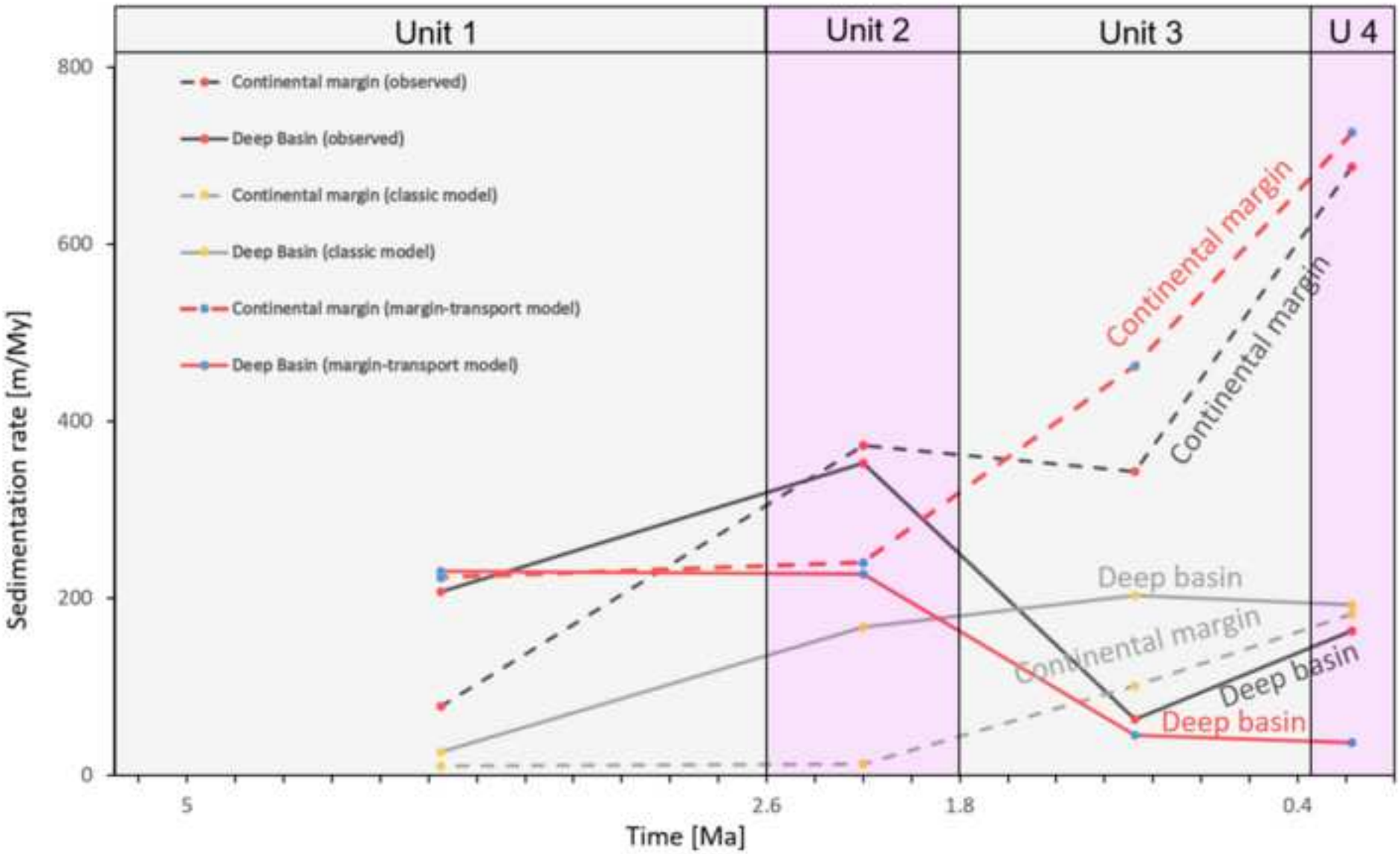

Figure 16

Click here to access/download;Figure;Fig 16.PNG

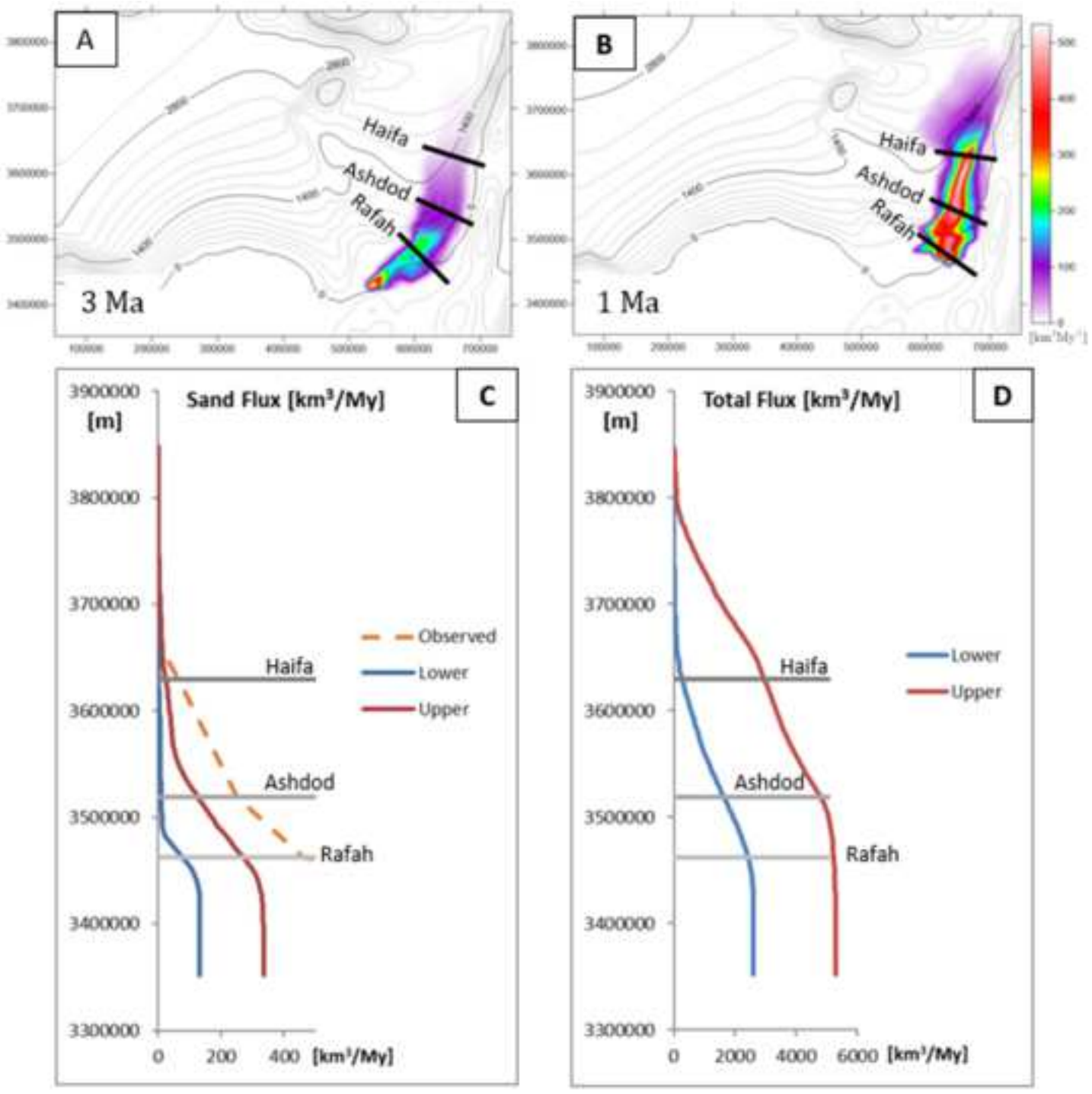

Figure 13

Click here to access/download;Figure;Fig 13 AR.PNG

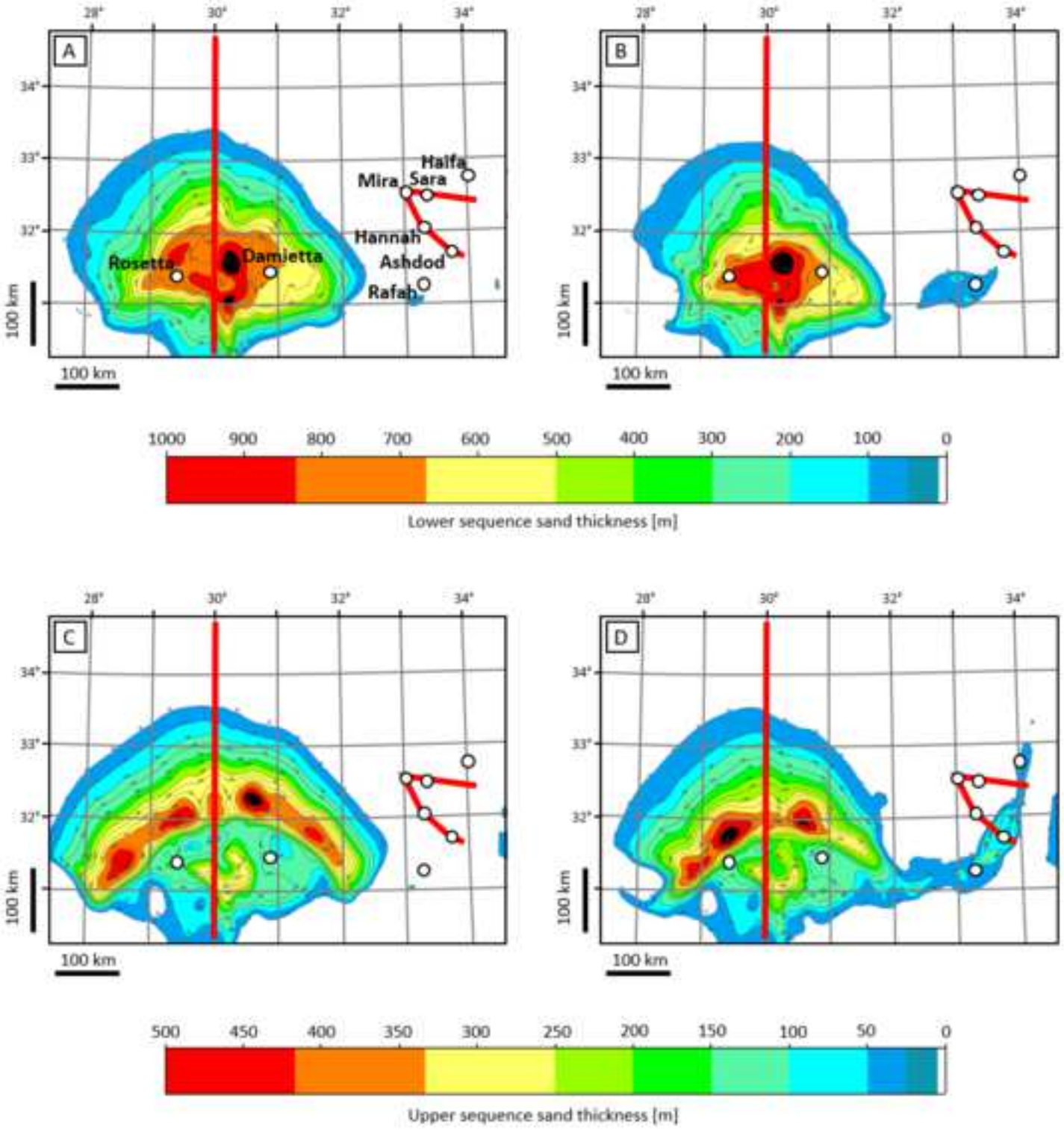

Figure 1

Click here to access/download;Figure;Fig 1 AR.PNG

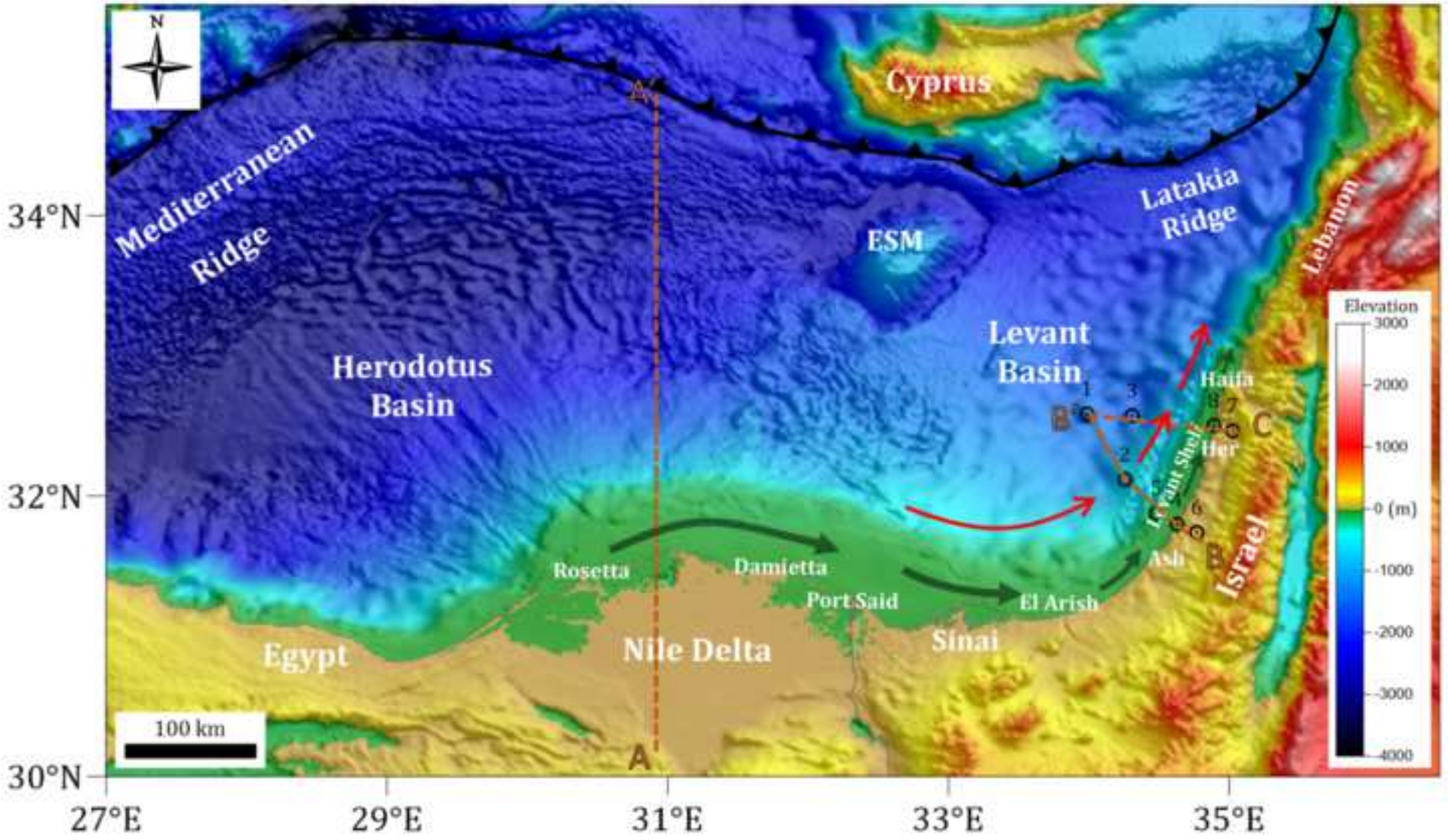

Figure 5

Click here to access/download;Figure;Fig 5 AR.PNG

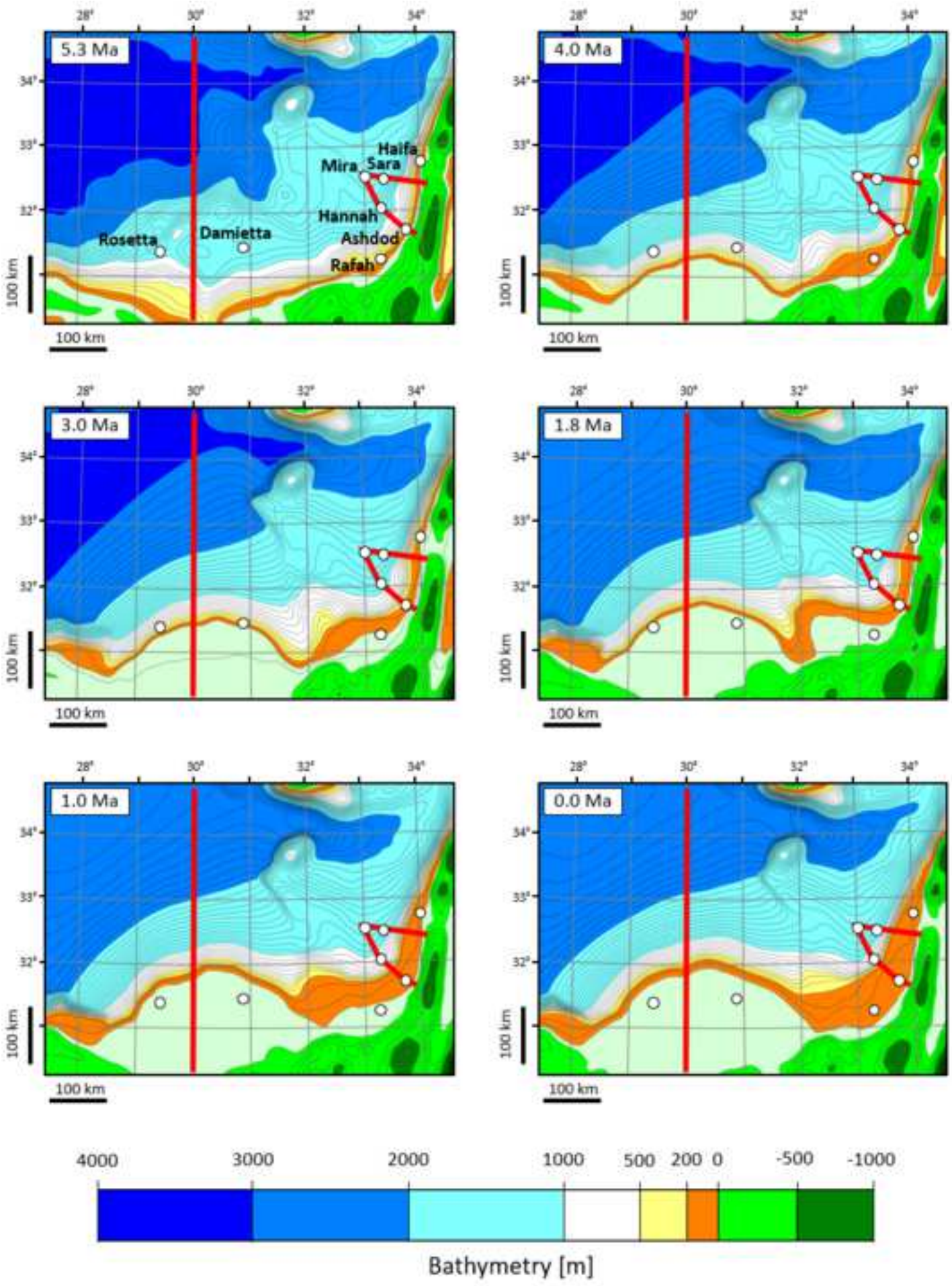

Figure 6

Click here to access/download;Figure;Fig 6 AR.PNG

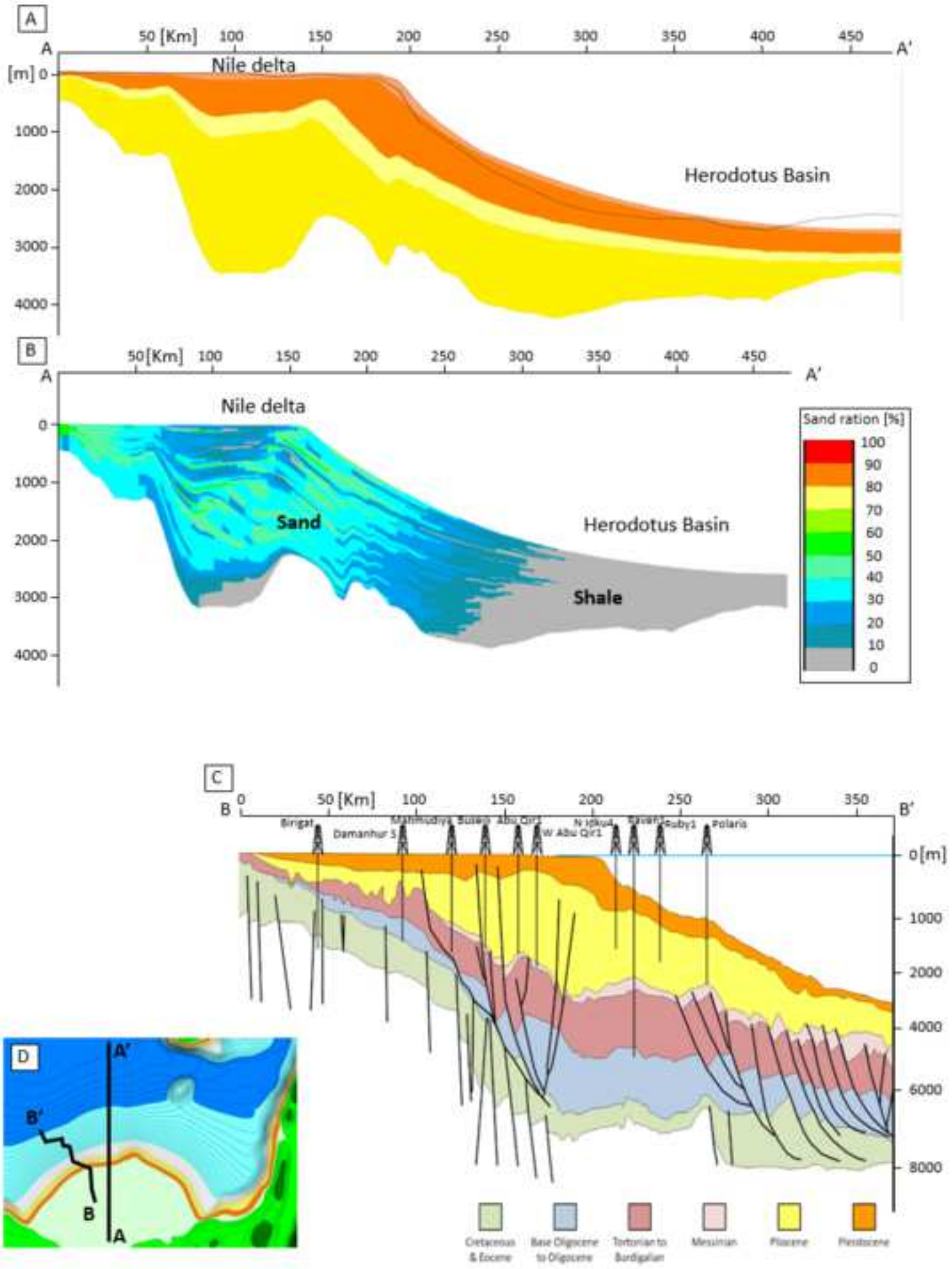

Figure 9

Click here to access/download;Figure;Fig 9 AR.PNG

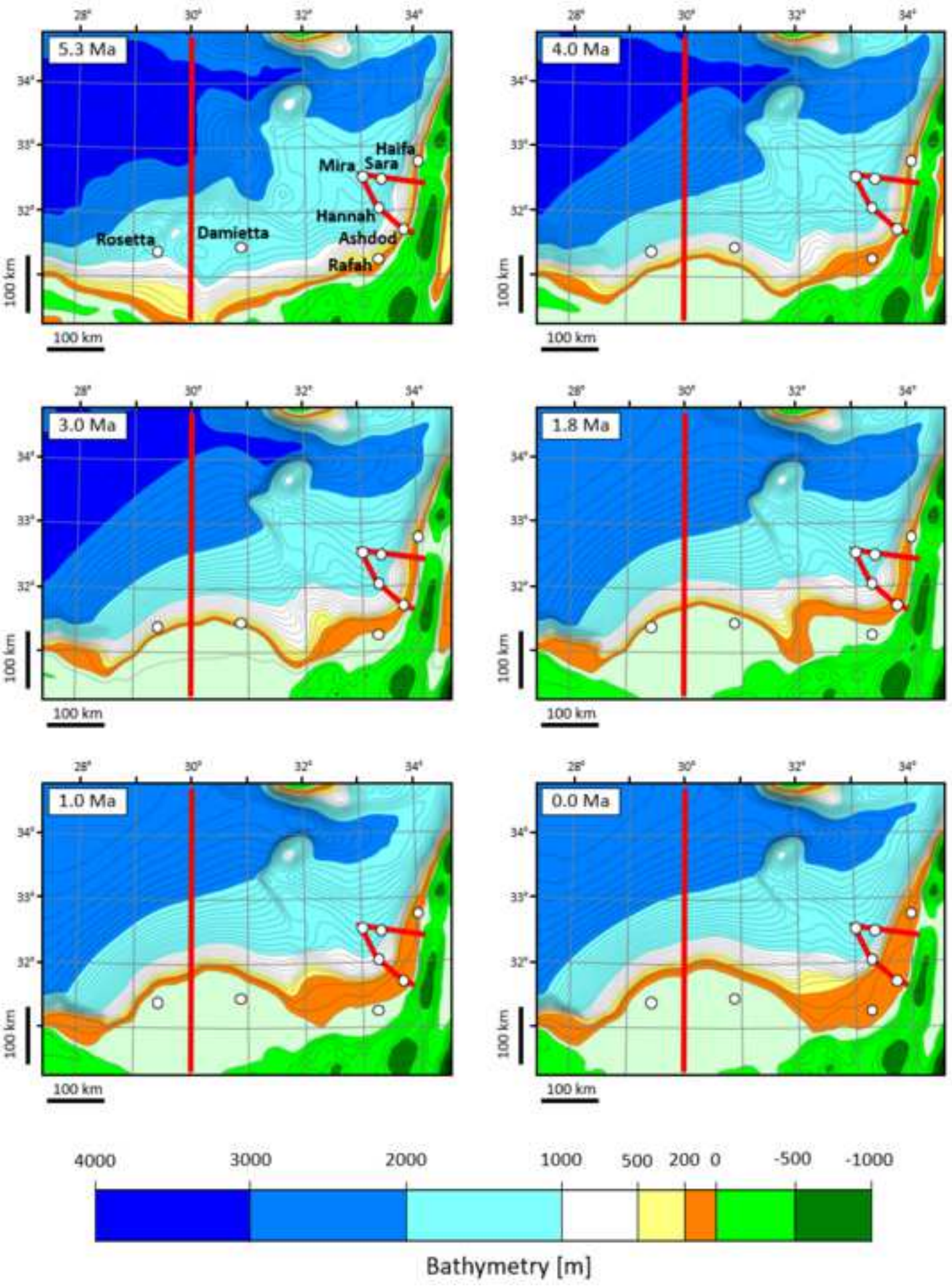

Table 1

Diffusion Coefficient [km²/ky]

Sand

		K gravity terrestrial [km²/ky]	K gravity marine [km²/ky]	K water terrestrial [km²/ky]	K water marine [km²/ky]
Csato et al., 2014	Delta	0.001	0.001	250	5
Zhang et al., 2018	Delta	0.05	0.005	50	0.01
Csato et al., 2013	Margin	0.001	0.001	2000	0.4
Harris et al., 2016	Margin	0.001	0.001	250	1
Gvirtzman et al., 2014	Turbidites	0.001	0.001	Not Defined	2
Hawie et al., 2017	Turbidites	0.001	0.001	Not Defined	0.3
Hawie et al., 2018	Turbidites	0.001	0.007	Not Defined	20
range		**0.001 - 0.05**	**0.001 - 0.005**	**50 - 2000**	**0.01 - 20**
Levant (this study)	**Delta and Margin**	**0.001**	**0.001**	**100**	**0.5**

Shale

		K gravity terrestrial [km²/ky]	K gravity marine [km²/ky]	K water terrestrial [km²/ky]	K water marine [km²/ky]
Csato et al., 2014	Delta	0.001	0.001	1000	5
Zhang et al., 2018	Delta	0.1	0.05	100	0.1
Csato et al., 2013	Margin	0.001	0.001	4000	10
Harris et al., 2016	Margin	0.001	0.001	1000	5
Gvirtzman et al., 2014	Turbidites	0.001	0.001	Not Defined	10
Hawie et al., 2017	Turbidites	0.001	0.001	Not Defined	0.063
Hawie et al., 2018	Turbidites	0.001	0.001	Not Defined	100
range		**0.001 - 0.1**	**0.001 - 0.05**	**100 - 4000**	**0.063 - 100**
Levant (this study)	**Delta and Margin**	**0.01**	**0.01**	**500**	**2.5**